https://doi.org/10.5194/essd-2026-344
Preprint. Discussion started: 19 August 2026

Open Access Earth System Science Data Discussions

CzechGrids Micro: microclimate temperature offset grids at 10 m resolution for the Czech Republic

Martin Macek[1*], Matěj Man[1*], Josef Brůna[1], Lucia Hederová[1,2], Tereza Klinerová[1], Jiří Prošek[1,3], Anna Růžičková[1], Jan Wild[1], Martin Kopecký[1]

1 Department of Geoecology, Institute of Botany of the Czech Academy of Sciences, Průhonice, 252 43 Czech Republic
2 Department of Phytology, Technical University in Zvolen, Zvolen, 960 01 Slovakia
3 Faculty of Environmental Sciences, Czech University of Life Sciences Prague, Kamýcká 129, Praha - Suchdol, CZ-165 00, Czech Republic

Correspondence to: Martin Macek (martin.macek@ibot.cas.cz)

*contributed equally

Abstract. Microclimate represents climatic conditions at spatial scales of meters to tens of meters and often deviates substantially from regional macroclimate due to effects of local topography and land cover. These deviations shape species distributions, ecosystem processes, and organism responses to climate change, yet spatially explicit microclimatic data have long been unavailable at national scales.

Here we present a high-resolution (10 m) dataset of monthly microclimatic temperature offsets for the Czech Republic. Microclimate is expressed as offsets between in situ air temperature measurements at 2 m height and downscaled, elevation-corrected macroclimatic temperatures from the ERA5-Land climate reanalysis. Temperature offsets were modelled separately for mean, minimum, and maximum monthly air temperature using generalized additive models trained on a large network of forest microclimate loggers and standard meteorological stations, covering the period 2018–2024. To capture spatially explicit microclimatic effects, the models integrated variables representing topographic parameters, vegetation characteristics, urban heat island effects and their seasonal dynamics.

The resulting CzechGrids Micro dataset consists of 39 GeoTIFF rasters providing monthly and annual local air temperature offsets that can be combined with downscaled ERA5-Land data to derive absolute microclimatic temperatures for any user-defined periods. The maps are primarily intended for applications in ecological research, climate impact assessments, and adaptation planning at fine spatial scales.

The CzechGrids Micro monthly temperature offset grids are freely available at: https://doi.org/10.5281/zenodo.18472086 (Macek et al., 2026)

https://doi.org/10.5194/essd-2026-344
Preprint. Discussion started: 19 August 2026

1. Introduction

Climate is a key environmental factor whose characteristics strongly depend on spatial scale. Most available climatic datasets describe macroclimate at meso- to macro-scales, typically ranging from kilometers to hundreds of kilometers. However, numerous studies have demonstrated the ecological importance of local climatic conditions at much finer spatial scales (meters to tens of meters), referred to as microclimate (De Frenne et al., 2013; Haesen et al., 2023b; Klinges et al., 2024; Macek et al., 2019).

Microclimatic conditions represent the immediate environmental context in which organisms live. Compared to macro- and mesoclimate, microclimate exhibits much finer spatial variability driven by land-surface topography (Ackerly et al., 2020; Ashcroft, 2006; Jucker et al., 2018; Macek et al., 2019), hydrology (Greiser et al., 2024; Von Arx et al., 2013), vegetation cover (Ehbrecht et al., 2019; Frey et al., 2016; Haesen et al., 2021; Rice et al., 2018; Zellweger et al., 2019), and other local drivers such as urban heat islands (Rizwan et al., 2008). At the landscape scale, microclimatic variation can exceed macroclimatic variability and directly influence species distributions, population dynamics, and organism physiology (Macek et al., 2019).

Due to its strong spatial heterogeneity, microclimate can substantially modify the impacts of climate change on biota, for example by buffering or amplifying these changes and by creating microrefugia that provide suitable conditions for survival and growth, thereby reducing the distances organisms must travel to track shifting climate (Ashcroft, 2010; Haesen et al., 2023a; Lenoir and Svenning, 2015). Despite its strong local variability, microclimate is not independent of macroclimate. Rather, it can be conceptualized as a macroclimatic background modified by local environmental drivers, such as topography and vegetation, which influence radiation balance, evapotranspiration (latent heat fluxes), and air flow. This perspective allows microclimate to be described as spatially structured offsets from large-scale climatic gradients (Haesen et al., 2021).

Reliable microclimatic maps are essential for modelling species distributions, interpreting and predicting climate change impacts, and planning adaptation measures (Haesen et al., 2023b; Lembrechts et al., 2019). Until recently, their availability for larger regions was limited by the scarcity of microclimatic measurements, the lack of predictors at appropriate spatial and temporal resolution, and high computational demands. Thanks to increasingly affordable standardized tools for microclimate measurements (Wild et al., 2019) and data-sharing networks (Lembrechts et al., 2020), substantial progress has been made in spatial microclimate modelling. However, available map products still struggle to simultaneously provide the spatial and temporal resolution, accuracy, and geographic coverage required for ecological applications (De Frenne et al., 2021; Potter et al., 2013; Uxa, 2025).

Here, we present high-resolution microclimatic air temperature grids for the Czech Republic, expressing local deviations from elevation-corrected macroclimate temperatures. The presented dataset builds on national weather station data combined with a dense network of in situ microclimatic measurements across the Czech Republic, with a particular focus on forest ecosystems, which strongly modify local climate yet are poorly represented in standard meteorological monitoring.

https://doi.org/10.5194/essd-2026-344
Preprint. Discussion started: 19 August 2026

To ensure consistency with large-scale climate, we expressed local temperature (microclimate) as an offset from the macroclimate, represented by air temperature from ERA5-Land reanalysis (Muñoz-Sabater et al., 2021). We modelled these microclimatic offsets using generalized additive models (GAM), following an empirical correlative approach with topographic, vegetation, and urban heat predictors. The resulting product comprises high-resolution (10 m) maps of mean monthly offsets for daily minimum, mean, and maximum air temperature at 2 m.

2 Methods

2.1 Study system

CzechGrids Micro dataset represents microclimatic air temperature of the Czech Republic (12° 05' E – 18° 52'' E; 48° 34' N – 51° 03' N; total area 78,866 km^2; Figure 1). Czech Republic is a landlocked country in Central Europe with a temperate climate, transitioning between Oceanic (Cfb) and Humid Continental (Dfb) climatic zones according to Köppen climate classification (Beck et al., 2018), with the long-term average of 8.3 °C for normal period 1991-2020 (Crhová et al., 2022). Elevations of natural surfaces vary between 115 and 1603 m a.s.l., and about 37 % of the area is forested.

2.2 Data sources

2.2.1 In situ temperature

Local climatic conditions are based on in situ measurements of air temperature at 2 m above ground level during the period 2018–2024. The input temperature dataset combines two types of measurements, representing variability of topography and land cover within the study area: microclimatic temperature observations primarily located within forest stands with diverse topographic context, and standard meteorological station measurements providing temperature data from non-forest environments (Figure 1, Figure 2).

Microclimatic observation dataset aggregates several networks with different coverage of geographic and environmental space (Table 1). Four national-level networks aim to regularly cover the whole country and elevation gradient and to represent different forest types regarding their structure and species composition. Four regional-level networks were designed to capture the main topographic gradients at the landscape scale within topographically diverse landscapes (elevation, topographic wetness, slope aspect). Finally, three intensive local-level networks aimed to capture fine-scale microclimatic variability linked to local topography and variations in vegetation cover. Microclimate temperature was measured every 15 minutes using Thermologger (TOMST s.r.o.), installed at a height of 2 m either on the northern side of a tree trunk (when available) or a pole and shielded by a single-layer plastic radiation screen. Each Thermologger is equipped with a DS7505U+ temperature sensor with a resolution of 0.0625 °C and an accuracy of ±0.5 °C.

https://doi.org/10.5194/essd-2026-344
Preprint. Discussion started: 19 August 2026

Standard weather station 2 m air temperature data measured at 10-minute intervals were obtained from a representative network of 257 stations covering the Czech Republic, using open data provided by the Czech Hydrometeorological Institute (CHMI; https://opendata.chmi.cz/). While most stations are intentionally located in flat, open terrain in accordance with the World Meteorological Organization recommendations (WMO, 2024), the dataset also includes stations in specific environments, such as exposed hilltops, urban areas, and sites affected by strong cold-air pooling in peatbogs or valley bottoms (Figure 2).

Data were quality-checked using supervised control procedure implemented in *myClim* R package (Man et al., 2023). Gaps in the raw time series shorter than one hour were filled by linear interpolation. The time series were then aggregated into daily mean, minimum and maximum, and subsequently into monthly averages of these variables using the *myClim* R package (Man et al., 2023). In addition, measurements from locations where forest structure had changed substantially since the period for which vegetation structure was estimated (2019-2021) were excluded. Finally, monthly air temperatures were used to calculate microclimate temperature offsets, defined as the differences between observed local air temperature and corresponding grid cell values from lapse-corrected ERA5-Land data (see Sect. 2.2.2).

Table 1 Overview of temperature loggers networks used in this study for model training. A total of 811 stations measuring 2 m air temperature with a cumulative record length of 4,083 years were used in this study.

Network type	Locality	Characteristics	Provider*	No. of stations	Period	Reference / source
National	Czechia	Standard weather stations	CHMI	257	2018 - 2024	https://opendata.chmi.cz/
	Czechia	Managed forests	IBOT	69	2018 - 2024	
	Czechia	Protected forests	IBOT	64	2020 - 2024	
	Czechia	Old-growth forests	LRI	22	2021 - 2024	pralesy.cz
Regional	České Středohoří	Volcanic landscape	IBOT	49	2018 - 2024	(Kopecký et al., 2024; Macek et al., 2019)
	Bohemian Switzerland NP	Sandstone landscape	IBOT	138	2018 - 2024	(Man et al., 2022a, b)
	Bohemian Karst	Karst landscape	IBOT	65	2018 - 2024	(Kopecký et al., 2024)
	Bohemian Forest NP	Mountain landscape	IBOT	100	2019 - 2024	(Brůna et al., 2026)
Local	Doutnáč Hill	Forest-grasslands mosaic on exposed slopes	IBOT	12	2024	
	Oblík Hill	Forest-grasslands mosaic on conic hill	IBOT	21	2024	
	Žofín Forest	Old-growth mixed fir-beech forest reserve	IBOT	13	2022 - 2024	

**IBOT = Institute of Botany of the Czech Academy of Sciences (Botanický ústav AV ČR); CHMI = Czech Hydrometeorological Institute (Český hydrometeorologický ústav), LRI = Landscape Research Institute (Výzkumný ústav pro krajinu).*

https://doi.org/10.5194/essd-2026-344
Preprint. Discussion started: 19 August 2026

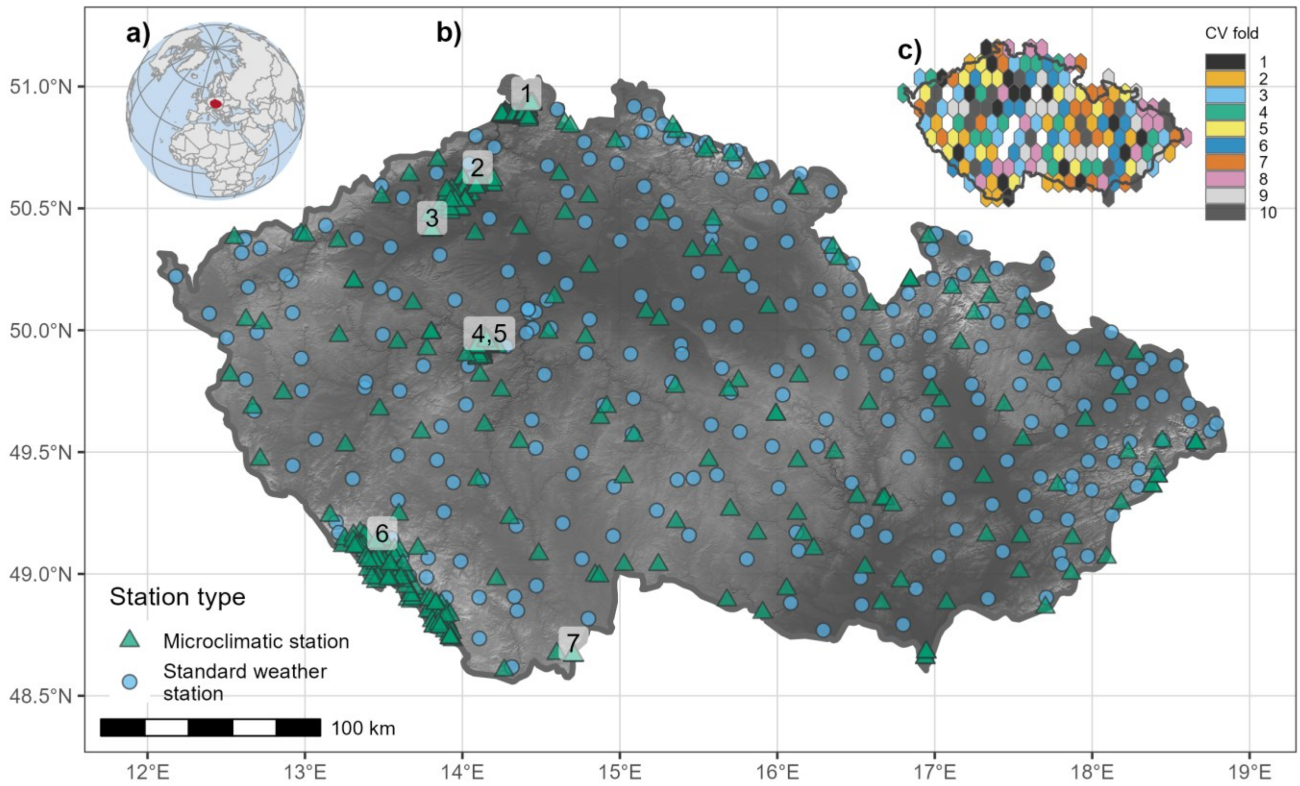

Figure 1 (a) Study area – Czechia, located in Central Europe. **(b)** The main map shows the locations of microclimate stations (green triangles) and weather stations (blue circles) used for temperature offset modelling. Shaded relief is plotted on the background. Regional/local microclimatic station networks: (1) Bohemian Switzerland NP, (2) České Středohoří, (3) Oblík Hill, (4) Bohemian Karst, (5) Doutnáč Hill, (6) Bohemian Forest NP, (7) Žofín Forest Reserve. **(c)** Hexagonal spatial blocks used for 10-fold spatial cross-validation; blocks are coloured according to the assigned fold.

2.2.2 Gridded macroclimate

Macroclimatic conditions were represented using the ERA5-Land global climate reanalysis (Muñoz-Sabater et al., 2021), which provides hourly meteorological data at a spatial resolution of 0.1° (~9 km) from 1950 to the present. Hourly air temperature at 2 m height was first aggregated to daily minimum, maximum, and mean values and then monthly averages were calculated for all months within the measurement period (2018–2024).

Next, monthly ERA5-Land temperatures were downscaled to the 10 m spatial resolution of CzechGrids Micro using empirically derived environmental lapse-rates to correct for differences in grid cell elevation between the native ERA5-Land grid and the target 10 m grid. Specifically, for each month and temperature variable, elevational lapse rates were estimated following the methodology of the Lapse Rate Based Temperature Downscaling tool (Conrad et al., 2015), using multiple regression between temperature, reference elevation from ERA5-Land grid, and second-order polynomial terms of spatial

https://doi.org/10.5194/essd-2026-344
Preprint. Discussion started: 19 August 2026

coordinates (Table B1). Reference elevation was calculated by dividing ERA5-Land geopotential height by the acceleration of gravity constant. Subsequently, temperatures were adjusted to sea-level using the empirically derived lapse rates applied to the reference elevation grid. Sea-level temperatures were then reprojected to 10 m spatial resolution (WGS84/UTM33N projection) using cubic spline interpolation implemented in *terra* R package (Hijmans, 2026). Finally, sea level temperatures were converted to temperatures at actual elevation using the same lapse rates in combination with local elevation from a 10 m digital terrain model (DTM; see chapter 2.2.3).

The resulting downscaled, lapse-rate corrected macroclimate grids served as the reference macroclimate for temperature offset calculation.

2.2.3 Topographic variables

To derive topographic variables representing terrain attributes relevant for microclimate modelling, we generated CzechGrids DTM - a digital terrain model with 10 m resolution derived from the LiDAR-based digital terrain model of the Czech Republic (DMR 5G; Czech Office for Surveying, Mapping and Cadastre). The DMR 5G is provided as a triangulated irregular network (TIN) point cloud with an average point spacing of 2 m in the S-JTSK / Krovak East North coordinate reference system (EPSG:5514).

First, we transformed the original point cloud to WGS84 / UTM33N coordinate reference system (EPSG:32633). We then generated a 2 m raster by interpolation based on Delaunay triangulation, implemented in the *lidR* R package (Roussel et al., 2020). The resulting 2 m grid was subsequently resampled to the target resolution of 10 m using B-spline interpolation in SAGA GIS (Conrad et al., 2015). Any remaining gaps in the DTM were filled using iterative smooth surface interpolation with the 'Close gaps' tool in SAGA GIS. High-resolution LiDAR DTMs contain human-made topographic depressions without surface outlet like quarries and these artificial depressions must be corrected before topographic analyses based on flow routing algorithms (Lindsay and Creed, 2006). To generate hydrologically corrected DTM, we first identified artificial depressions using DepthInSink tool in Whitebox Tools 2.4.0 (Lindsay, 2016) and then replaced the elevation of the lowest cell of each depression by NA value to allow the digital flow routing algorithm to drain water from the sink. Subsequently, we filled the remaining topographic depressions using a hybrid algorithm combining filling of single-cell sinks and breaching of larger depressions (Lindsay and Dhun, 2015). Together, this workflow maintained the topography of the real depressions within the landscape and simultaneously ensured the minimum alteration of the resulting hydrologically corrected DTM.

From the resulting CzechGrids DTM, we extracted *elevation* and derived following microclimate-relevant topographic variables using SAGA GIS 9.8.0 (Conrad et al., 2015):

Slope characterizes terrain steepness in angular degrees. It enters subsequent calculations of moisture-related parameters and influences irradiance. Slope was calculated using the second-order polynom method (Zevenbergen and Thorne, 1987).

Aspect describes slope orientation in degrees. It affects irradiance as well as exposure to wind and precipitation.

https://doi.org/10.5194/essd-2026-344
Preprint. Discussion started: 19 August 2026

Sky view factor represents the degree of sky obstruction by the surrounding terrain. This parameter is important for the local energy balance, particularly because it influences both incoming and outgoing radiation. Sky view factor was calculated following (Böhner and Antonić, 2009), using 32 azimuth directions within a 10 km radius.

Topographic wetness is a dimensionless index expressing the potential moisture conditions of a site, and it is a useful proxy also for cold air pooling (Macek et al., 2019; Vanwalleghem and Meentemeyer, 2009). Here, we used SAGA Wetness Index, which better reflects cold air pooling in topographically flat terrain depressions (Böhner and Antonić, 2009). Following recommendation (Kopecký et al., 2021), we used Freeman multiple-flow routing, local slope and suction parameter value of 10.

Distance to channel represents the site's height above the channel network. It was calculated as a difference between the elevation of a given grid cell and a smooth surface interpolated from channel network elevations using B-spline interpolation. Distance to channel is therefore a variant of the widely used height above the nearest drainage (Nobre et al., 2011), but with the advantage of smooth transitions between watersheds. For microclimatic offset modelling, values were left-censored at zero to ensure positive values and subsequently square-root transformed.

Wind exposition quantifies the topographic exposure of a site. It accounts for the relative position with respect to the surrounding terrain within a 10 km radius and indicates the degree to which a site is ventilated, with values below 1 indicating sheltered locations and values above 1 indicating wind-exposed locations (Böhner and Antonić, 2009).

2.2.4 Vegetation characteristics

Vegetation was characterized by *Canopy height, Tree cover,* and *Evergreen cover.*

Canopy height was derived from the Meta–WRI Global Canopy Height Model (Meta-CHM) (Tolan et al., 2024). Meta-CHM provides global estimates of canopy height above ground at sub-meter spatial resolution, derived primarily from 2019–2020 Maxar satellite imagery using self-supervised deep learning models trained on aerial and GEDI LiDAR data. For microclimate modelling, we reprojected the Meta–CHM to a target 10 m resolution using median aggregation. Several tiles of the Meta–CHM contained gaps due to clouds. To fill these gaps, covering ca 0.25 % of the study area, we used canopy height from national photogrammetry-based canopy height model for years 2021-2022 (NLI-CHM; Czech Forestry Institute, https://nli.gov.cz), adjusted via a zero-intercept linear regression between the Meta–CHM and NLI-CHM, and merged using a 30 m smoothing transition to produce a seamless canopy height model for the study area (*Canopy height*).

Tree cover was defined as the proportion of grid cells with *Canopy height* > 2 m calculated at two scales to account for edge effects by applying 50 m and 100 m Gaussian filters on the binary tree cover grid, creating *Tree cover 50 m* and *Tree cover 100 m*, respectively.

Evergreen cover was derived from the seasonal differences in the Normalized Difference Vegetation Index (NDVI). NDVI was calculated from harmonized Sentinel-2 Level-2A multispectral surface reflectance imagery at 10 m spatial resolution. Specifically, we used atmospherically corrected surface reflectance data from Sentinel-2 (COPERNICUS/S2_SR_HARMONIZED) and applied a two-step quality filtering procedure in Google Earth Engine

https://doi.org/10.5194/essd-2026-344
Preprint. Discussion started: 19 August 2026

(Gorelick et al., 2017). First, we masked pixels with cloud probability ≥ 25 % using the Sentinel-2 cloud probability dataset (COPERNICUS/S2_CLOUD_PROBABILITY). Second, we applied an edge mask based on the 20 m and 60 m bands to remove unreliable pixels near scene borders. Finally, NDVI was computed as the normalized difference between the NIR (Band 8) and red (Band 4) bands over the three-year period 2019–2021, corresponding to the vegetation state captured by the canopy height model.

To derive *Evergreen cover*, we used seasonal differences between median NDVI from the growing season (May–September) and the winter season (October–April). These differences were rescaled to a unit interval using a logistic transformation, with the inflection point (θ = -0.199) estimated from the histogram of NDVI differences using Otsu's classification. Non-forest areas, defined as pixels with canopy height < 2 m, were assigned zero values. A 20 m Gaussian filter was subsequently applied to reduce noise and account for edge effects. Thresholding and subsequent raster processing were performed using the *autothresholdR* (Landini et al., 2017) and *terra* (Hijmans, 2026) R packages. A workflow overview and additional processing details are provided in Appendix A.

2.2.5 Urban heat islands

Night-time light intensity (***Nightlights***) was used as a proxy for urban heat island effects (Rizwan et al., 2008; Song et al., 2021). *Nightlights* were derived as the square-root–transformed median night-time light intensity for the period 2014–2022 from the NASA/NOAA VIIRS dataset (Elvidge et al., 2021). The data were subsequently resampled from the original 500 m spatial resolution to the target 10 m resolution using cubic spline interpolation in *terra* R package.

https://doi.org/10.5194/essd-2026-344
Preprint. Discussion started: 19 August 2026

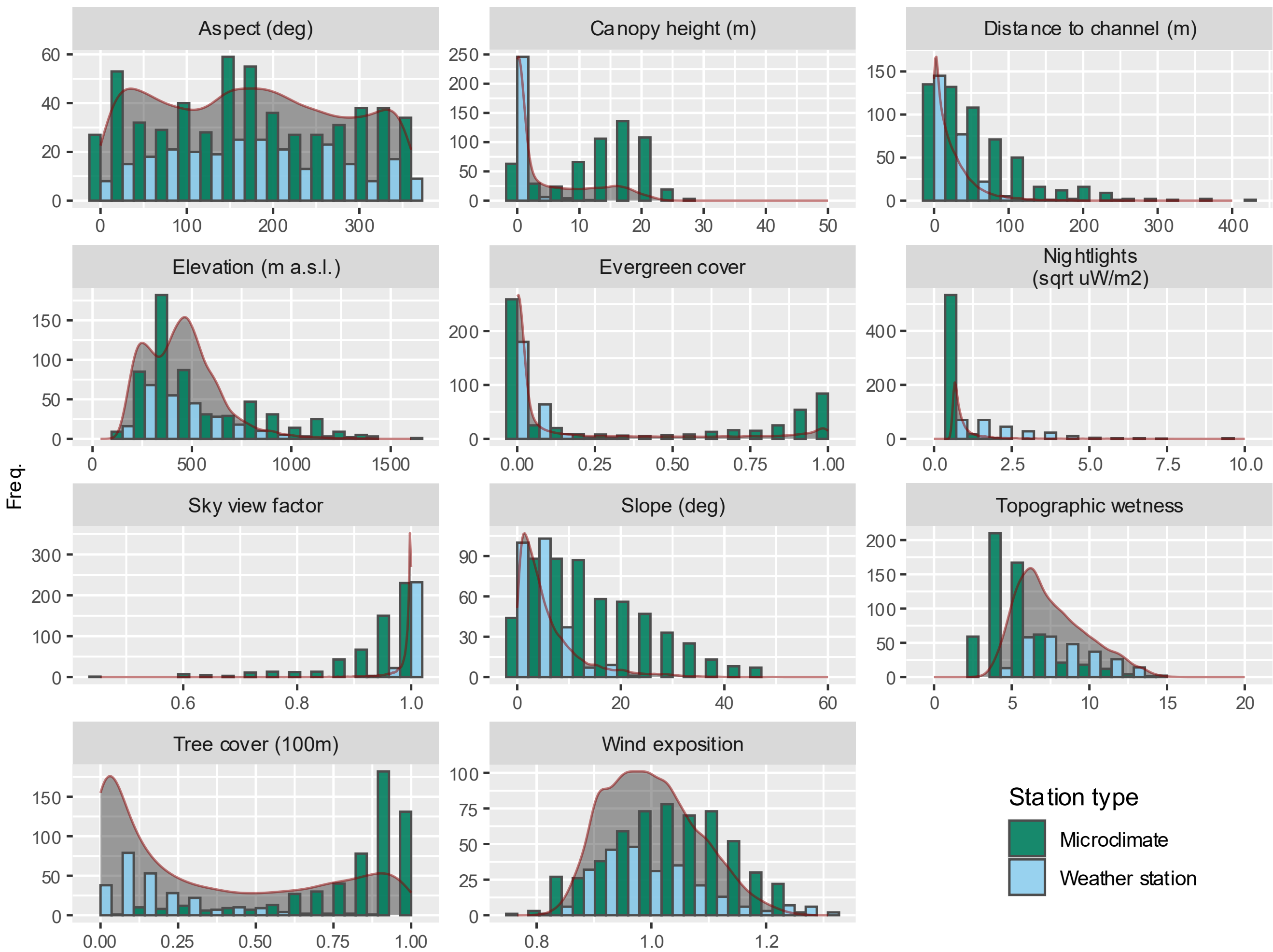

Figure 2 Distribution of microclimate and weather stations along gradients of predictor variables. The gray-shaded area represents the density distribution of these variables across the entire study area. While microclimate stations represent air temperatures mostly from forests and capture also topographically extreme sites with steeper slopes and lower sky view factors, weather stations represent mostly treeless habitats in topographically less exposed sites and sites affected by urban heat islands.

2.3 Modelling microclimate offsets

2.3.1 Model training

To model microclimatic offsets—defined as the differences between measured monthly values and the downscaled ERA5-Land reanalysis—we used Generalized Additive Models (GAMs) implemented via the '*bam*' function in the *mgcv* R package (Wood et al., 2017). The *bam* function is optimized for large datasets and fits models using fast restricted maximum likelihood

https://doi.org/10.5194/essd-2026-344
Preprint. Discussion started: 19 August 2026

Open Access Earth System Science Data Discussions

(fREML). This framework enables flexible modelling of nonlinear relationships with data-driven smoothness selection, reducing overfitting and limiting implausible response shapes.

The response variables were the monthly microclimatic offset for mean, minimum, and maximum air temperature, with each metric modelled separately. All models were fitted using data from the full annual cycle. Seasonal variation in microclimatic offsets was modelled by cyclic cubic regression splines for the month variable, which ensured continuity of the fitted effect between December and January. Month was included both as a main effect and in interaction with all other smooth covariates using tensor product interaction, allowing the effects of predictors to vary seasonally.

The effect of slope exposure was modelled by a tensor product smooth for *Slope* and *Aspect*, with a thin plate regression spline basis for *Slope* and a cyclic cubic regression spline basis for *Aspect* (0–360°), and their tensor product interaction with *month* represented by a cyclic cubic regression spline. This formulation allowed estimation of seasonally variable anisotropic radiative heating effects while ensuring continuity at the 0°-360° aspect boundary, up to the second derivative.

Although the correction for elevation was already incorporated during ERA5-Land downscaling, the actual lapse rate may differ slightly from the lapse rate inherited from the ERA5-Land reanalysis. *Elevation* was therefore included in the model as a smooth predictor interacting with month to account for residual adiabatic effects.

Remaining predictors included topographic parameters (*Distance to channel*, *Topographic wetness, Sky view factor,* and *Wind exposition)*, urban heat islands (*Nightlights),* and vegetation characteristics (*Canopy height*, *Forest cover 50 m* and *Forest cover 100 m*, and *Evergreen cover*). These effects were modelled using thin-plate regression splines with additional shrinkage penalty, allowing the entire smooth term to shrink toward zero when unsupported by data (Marra and Wood, 2011).

To capture phenological effects, *Canopy height* and *Evergreen cover* were also included in three-way interaction with month. Models assumed normally distributed errors and included random effects for site and calendar month to account for repeated sampling and temporal autocorrelation. To limit wiggliness of smooth functions to physically plausible shapes while maintaining computational efficiency, we limited the maximal basis dimension for smooth terms to $k = 5$. To reduce overfitting and partially account for temporal autocorrelation, we increased the gamma parameter to 21.66, corresponding to one third of the median temporal sample size per station.

Spatial autocorrelation was addressed through site-specific weights based on kernel estimates of spatial sampling density, thereby down-weighting the influence of clustered observations. Specifically, for each calendar month, we calculated local site density using a Gaussian kernel with bandwidth $\sigma = 2.5$ km applied on pairwise Euclidean distances among sites, and used the inverse of this density as observation weights in the GAM model.

Finally, we produced the final reduced models from the full models by removing strongly penalized terms (empirical degrees of freedom < 0.5 for main effects and < 1.5 for interaction terms) as well as statistically non-significant terms ($p > 0.05$). These reduced models were then refitted without extra shrinkage penalization of smooth terms. Removing strongly penalized terms had little effect on the model fit but substantially reduced the computational demands for spatial prediction. To visualize partial effects, we used R packages *ggplot2* (Wickham, 2016), and *gratia* (Simpson, 2024).

https://doi.org/10.5194/essd-2026-344
Preprint. Discussion started: 19 August 2026

Open Access Earth System Science Data Discussions

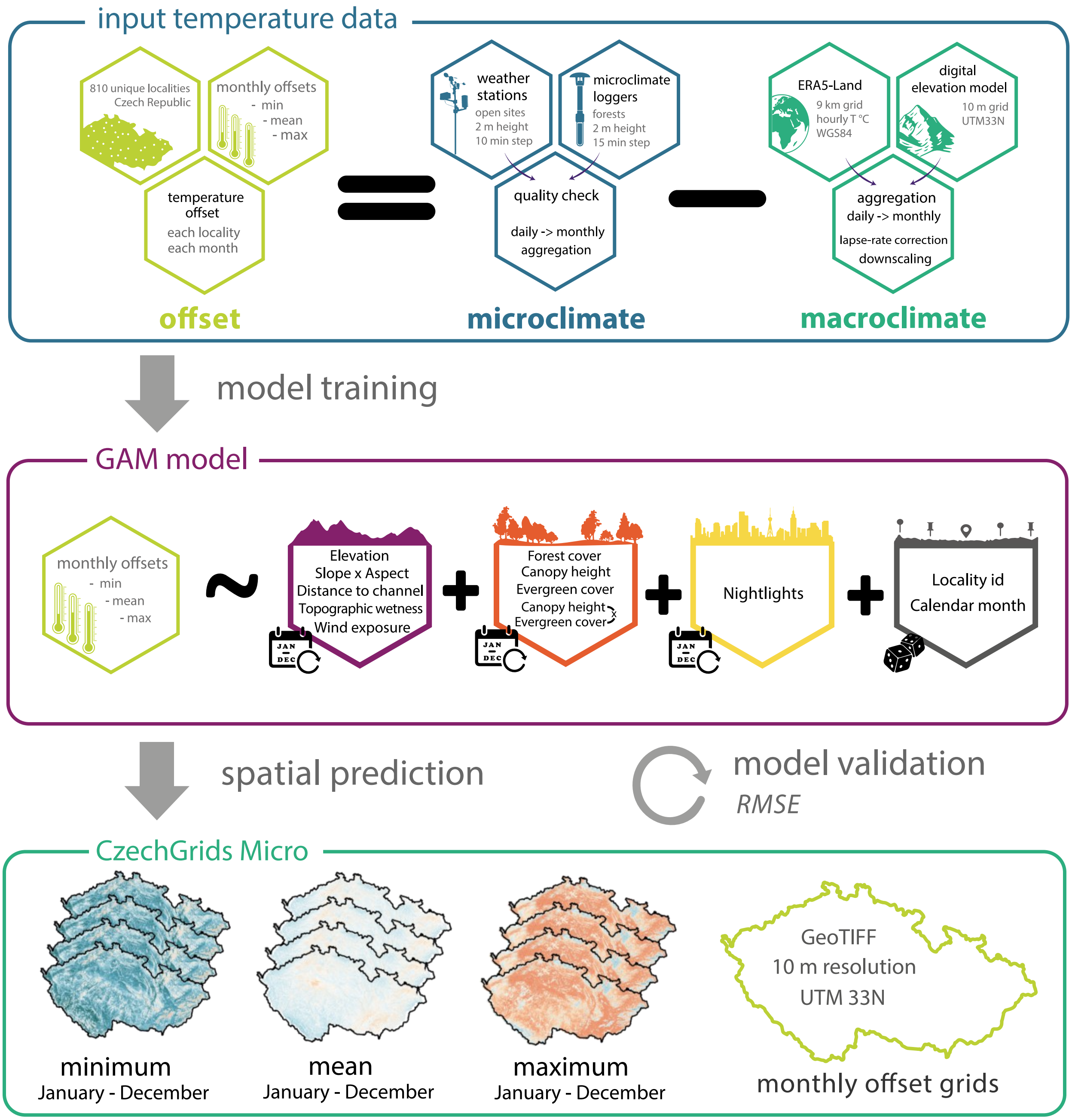

Figure 3 Schematic overview of the modelling workflow, including climate data processing (top), generalized additive model (GAM) structure and validation (middle), and spatial raster prediction of monthly microclimate offsets at 10 m resolution (bottom). Predictors included in the GAM model are grouped into thematic categories representing topography, vegetation structure, urbanization, and random effects.

https://doi.org/10.5194/essd-2026-344
Preprint. Discussion started: 19 August 2026

2.3.2 Model validation

We used 10-fold spatial block cross-validation (CV) to quantify the predictive performance of the final model trained on spatially structured data. The study area was divided into a regular hexagonal grid with a cell size of 30 km (n = 172), and cells were assigned into ten folds (Figure 1c) using a constrained randomization procedure to balance the number of localities per fold implemented in the *blockCV* R package (Valavi et al., 2019). In each of ten CV iterations, one fold was withheld from model training and used for independent evaluation. Predictive accuracy was then assessed using the root mean squared error (RMSE), calculated over observations across all CV folds as:

$$\mathrm{RMSE} = \sqrt{\frac{1}{N}\sum_{i=1}^{N}(y_i - \hat{y}_i)^2}$$

where y_i is the observed value and $\hat{y}_i$ is the predicted value.

We calculated RMSE separately for each month as well as across all months combined. In addition, RMSE was evaluated for the complete dataset and separately for subsets corresponding to microclimatic stations and weather stations.

2.3.3 Spatial prediction

To generate gridded monthly microclimatic offsets at 10 m spatial resolution for the whole Czech Republic, we applied the final GAM models to the national-scale gridded predictors. Because the models were trained using both weather stations and microclimate stations, the station-type predictor was fixed to "weather station" during spatial prediction to ensure consistent predictions across the study area. Random effects included during model fitting to account for data structure were excluded from prediction, yielding population-level offset estimates. Predictions were computed for each month in parallelized tiles and subsequently merged into seamless raster grids, stored as cloud-optimized GeoTIFFs with Limited Error Raster Compression (LERC_ZSTD) with an accuracy of 0.005 K. Annual offsets were then calculated as the average of the 12 monthly layers.

Finally, we evaluated the physical plausibility of the resulting grids (Uxa, 2025). First, we calculated absolute temperatures by adding microclimatic offsets to downscaled monthly aggregated macroclimate data (2018–2024 mean). Then, we verified that predicted monthly minimum temperatures were lower than mean temperatures, and mean temperatures were lower than maximum temperatures in every grid cell.

All computations were performed in R 4.5.2 (R Core Team, 2025) using *terra* package.

https://doi.org/10.5194/essd-2026-344
Preprint. Discussion started: 19 August 2026

Open Access Earth System Science Data Discussions

3 Results

In total, we used 48,999 monthly offsets for each variable (T_{MIN}, T_{MEAN}, T_{MAX}) from 810 unique localities for model training. Observed monthly offsets ranged between -8.8 and +8.02 K, with overall means within 1 K from downscaled macroclimate for all variables and locality types (Table 2).

Table 2 Summary statistics of monthly offsets (in Kelvins) between downscaled macroclimate temperatures and in-situ measured temperatures. The statistics were calculated separately for maximum, mean, and minimum temperature offsets, and by station type (microclimate vs. weather stations). While microclimate stations measured mostly in forest understory, weather stations represent open treeless habitats.

Offset	Station	Mean	Median	SD	Min	Max
T_{MIN}	Microclimate	-0.59	-0.36	1.41	-8.8	3.43
	Weather station	-1.00	-0.86	1.40	-8.57	4.02
	All	-0.77	-0.57	1.43	-8.8	4.02
T_{MEAN}	Microclimate	-0.60	-0.49	0.89	-5.68	2.40
	Weather station	-0.18	-0.13	0.69	-3.77	2.75
	All	-0.42	-0.32	0.84	-5.68	2.75
T_{MAX}	Microclimate	-0.15	-0.33	1.45	-6.26	8.02
	Weather station	0.76	0.77	0.80	-3.11	3.77
	All	0.24	0.27	1.29	-6.26	8.02

Model performance

Microclimate models showed good explanatory power for all variables, with adjusted R^2_{Tmin}= 0.822, adj. R^2_{Tmean}= 0.712, and adj. R^2_{Tmax}= 0.713. Spatial cross-validation RMSE was lowest for T_{MEAN}, ranging between 0.51 and 0.65 K for individual months, and highest for T_{MIN} with RMSE values between 0.70 and 1.15 K (Table 3).

Table 3 RMSE (in Kelvins) from 10-fold spatial cross-validation for microclimatic offset models. Monthly RMSE values were calculated by pooling observations by calendar month (1-12) by aggregating data from the same month over all years. The overall RMSE for all months was calculated from the full dataset and for subsets for microclimatic station only and weather station only.

Month:	1	2	3	4	5	6	7	8	9	10	11	12	Microclimate stations	Weather stations	Overall
RMSE T_{MIN}	0.88	0.95	1.03	1.12	1.08	1.06	1.15	1.08	1.15	1.01	0.77	0.70	1.03	0.98	1.01
RMSE T_{MEAN}	0.56	0.65	0.61	0.56	0.55	0.56	0.59	0.60	0.61	0.60	0.55	0.51	0.61	0.53	0.58
RMSE T_{MAX}	0.63	0.77	0.87	0.90	1.01	1.1	1.14	1.1	0.92	0.74	0.75	0.64	1.07	0.59	0.90

Microclimatic offsets were jointly controlled by seasonality, topography, vegetation characteristics, and urban heat islands, but strength and shape of individual effects strongly differed among temperature minima, means, and maxima (Table 4, Figure B1-B3). Month was a dominant temporal predictor across all models, with the main effect showing high F-statistics and

https://doi.org/10.5194/essd-2026-344
Preprint. Discussion started: 19 August 2026

Open Access Earth System Science Data Discussions

moderate nonlinearity (edf ≈ 2.8), indicating consistent but nonlinear seasonal variation in temperature offsets. Interactions between month and other topographic and vegetation terms also showed strong seasonal modification

Land-surface topography strongly affected microclimatic offsets (Table 4). Elevation was consistently selected in all fitted models, which suggests that the empirical lapse-rate correction based on ERA5-Land (Table B1) did not completely account for adiabatic temperature lapse signal in the microclimatic offsets.

Besides elevation, other topographic variables affected all modelled variables. Minimum temperature offsets were driven by cold-air pooling in sheltered topographic depressions as represented by *Wind exposition, Topographic wetness, and Distance to channel* (Table 4, Figure C1). Mean temperature offsets were controlled mostly by *Wind exposition and Distance to channel* and less by *Sky view factor* and *Slope × Aspect* (Table 4, Figure C2). Maximum temperature offsets were controlled mostly by *Sky view factor* and complex interaction of *Slope × Aspect*, but all remaining topographic variables also showed significant, but weaker effects (Table 4, Figure C3).

Vegetation characteristics showed consistent - but generally weaker - effects than topography, often with seasonal interactions, indicating that vegetation effects vary throughout the year, depending on vegetation phenology. While minimum temperatures were most strongly affected by *Canopy height, Forest cover* affected mean and maximum temperature offsets, but not minimum temperature. In contrast, *Evergreen cover* had a strong, but seasonally variable effect on all three temperature variables.

Urban heat islands, represented by *Nightlight* intensity, had strong effects on minimum and mean temperature offsets but not on maximum temperatures, suggesting localized nocturnal warming effects typical of built-up environments (Table 4, Figures C1-3). This anthropogenic influence on microclimate offsets was persistent through the year, because seasonal interactions with nightlights were only modest.

Partial effect of microclimatic station was estimated to be -0.52 ± 0.03 K for minimum, -0.32 ± 0.02 K for mean, and 0.23 ± 0.02 K for maximum temperatures compared to weather station temperatures.

https://doi.org/10.5194/essd-2026-344
Preprint. Discussion started: 19 August 2026

Table 4 Predictors included in the final reduced generalized additive models (GAMs) for minimum (T_{MIN}), mean (T_{MEAN}), and maximum (T_{MAX}) air temperature offsets. Predictors are grouped by category (time, topographic, vegetation, other environmental variables, and random effects). Reported values represent the effective degrees of freedom (edf) and F-statistics of smooth terms. Tensor-product interaction terms with month indicate seasonal modulation of predictor effects. Dashes (–) denote predictors not retained in the respective model. All smooth terms selected in reduced models were statistically significant ($p < 0.001$). Random effects account for repeated measurements within localities and temporal autocorrelation.

Predictor type	Predictor	T_{MIN} offset (edf / F)	T_{MEAN} offset (edf / F)	T_{MAX} offset (edf / F)
Time	Month	2.82 / 14268.9	2.87 / 9005.1	2.80 / 7166.9
Topographic	Distance to channel	0.84 / 258.1	1.02 / 367.9	0.94 / 91.4
	Distance to channel × Month	–	–	2.01 / 17.2
	Elevation	2.64 / 5917.2	3.32 / 7074.6	3.67 / 2622.3
	Elevation × Month	2.78 / 47.0	3.69 / 201.3	5.60 / 225.6
	Sky view factor	–	0.99 / 237.6	1.06 / 416.2
	Sky view factor × Month	–	–	1.81 / 12.0
	Slope × aspect	1.19 / 286.8	4.59 / 150.3	9.20 / 243.0
	Topographic wetness	3.67 / 1382.2	–	2.89 / 195.0
	Wind exposition	2.81 / 19411.1	2.89 / 5928.4	0.87 / 57.2
	Wind exposition × Month	4.76 / 425.1	3.97 / 310.2	–
Vegetation	Canopy height	1.33 / 2085.9	0.70 / 36.3	1.17 / 313.2
	Canopy height × Month	2.99 / 146.7	–	5.50 / 74.0
	Evergreen cover	0.96 / 802.1	0.95 / 382.0	0.68 / 23.6
	Evergreen cover × Month	2.45 / 43.8	2.79 / 46.6	3.39 / 352.1
	Forest cover 50m	–	–	2.96 / 360.7
	Forest cover 50m × Month	–	3.04 / 106.3	2.42 / 15.9
	Forest cover 100m	–	0.77 / 78.5	–
	Forest cover 100m × Month	–	–	–
Urban heat islands	Nightlights	2.41 / 4938.8	1.02 / 2235.3	–
	Nightlights × Month	2.08 / 26.2	1.88 / 16.4	–
Random effects	Month of measurement	65.2 / 94.2	53.6 / 43.2	61.2 / 67.3
	Locality ID	383.7 / 43.5	305.3 / 23.7	190.4 / 9.0

Spatial predictions at 10 × 10 m resolution were generated for the entire Czech Republic, comprising 789 million grid cells, for 3 × 12 monthly layers and three annual layers (Figure 4, Table 5). The range of predicted values across the continuous grids remained within the variability observed at the localities used for model training (cf. Table 2 and Table Table 5). Microclimatic minimum temperature offsets were, on average, 0.88 K lower than macroclimatic minimum temperatures. Mean temperature offsets were close to zero (-0.26 K), whereas microclimatic maximum temperatures were higher than macroclimatic temperatures (+0.46 K). For visualization of all 39 layers, see Supplementary figures S1-39.

https://doi.org/10.5194/essd-2026-344
Preprint. Discussion started: 19 August 2026

Table 5 Summary statistics for modelled monthly and annual microclimatic temperature offsets for the Czech Republic (789,084,655 unique raster cells). The microclimatic offsets were calculated as the difference between locally measured air temperature at 2 m above ground and lapse rate corrected 2 m temperature estimates from ERA5-Land climate reanalysis.

	TMIN					TMEAN					TMAX				
Month	**Mean**	**Median**	**SD**	**Min**	**Max**	**Mean**	**Median**	**SD**	**Min**	**Max**	**Mean**	**Median**	**SD**	**Min**	**Max**
1	-0.14	-0.20	0.50	-2.34	3.66	-0.01	-0.01	0.18	-3.13	1.20	-0.09	0.16	0.56	-5.94	1.45
2	-0.11	-0.16	0.58	-2.60	3.89	0.09	0.08	0.24	-3.16	1.46	0.12	0.32	0.55	-5.68	1.67
3	-0.36	-0.43	0.77	-3.52	4.16	0.06	0.05	0.34	-3.46	1.92	0.46	0.66	0.63	-5.34	2.11
4	-0.74	-0.83	0.93	-4.39	4.28	-0.05	-0.05	0.41	-3.74	2.15	0.80	0.99	0.65	-4.93	2.46
5	-1.10	-1.21	0.97	-4.84	4.21	-0.19	-0.19	0.38	-3.86	1.94	1.04	1.22	0.61	-4.55	2.67
6	-1.41	-1.54	0.96	-5.05	4.00	-0.35	-0.35	0.35	-3.94	1.75	1.12	1.36	0.64	-4.87	2.90
7	-1.64	-1.77	0.98	-5.28	3.71	-0.52	-0.52	0.37	-4.13	1.56	1.02	1.31	0.73	-5.17	2.95
8	-1.71	-1.85	1.02	-5.46	3.43	-0.66	-0.67	0.41	-4.39	1.48	0.75	1.07	0.79	-5.39	2.56
9	-1.56	-1.68	0.99	-5.22	3.24	-0.69	-0.70	0.43	-4.46	1.42	0.41	0.75	0.82	-5.67	2.26
10	-1.11	-1.21	0.83	-4.28	3.21	-0.53	-0.53	0.35	-4.11	1.24	0.11	0.44	0.77	-6.02	1.89
11	-0.54	-0.62	0.61	-3.04	3.34	-0.25	-0.25	0.24	-3.54	1.11	-0.09	0.22	0.66	-6.07	1.56
12	-0.14	-0.20	0.50	-2.34	3.66	-0.01	-0.01	0.18	-3.13	1.20	-0.09	0.16	0.56	-5.94	1.45
Annual	**-0.88**	**-0.97**	**0.80**	**-4.02**	**3.72**	**-0.26**	**-0.26**	**0.31**	**-3.76**	**1.49**	**0.46**	**0.70**	**0.63**	**-5.34**	**2.11**

https://doi.org/10.5194/essd-2026-344
Preprint. Discussion started: 19 August 2026

Open Access Earth System Science Data Discussions

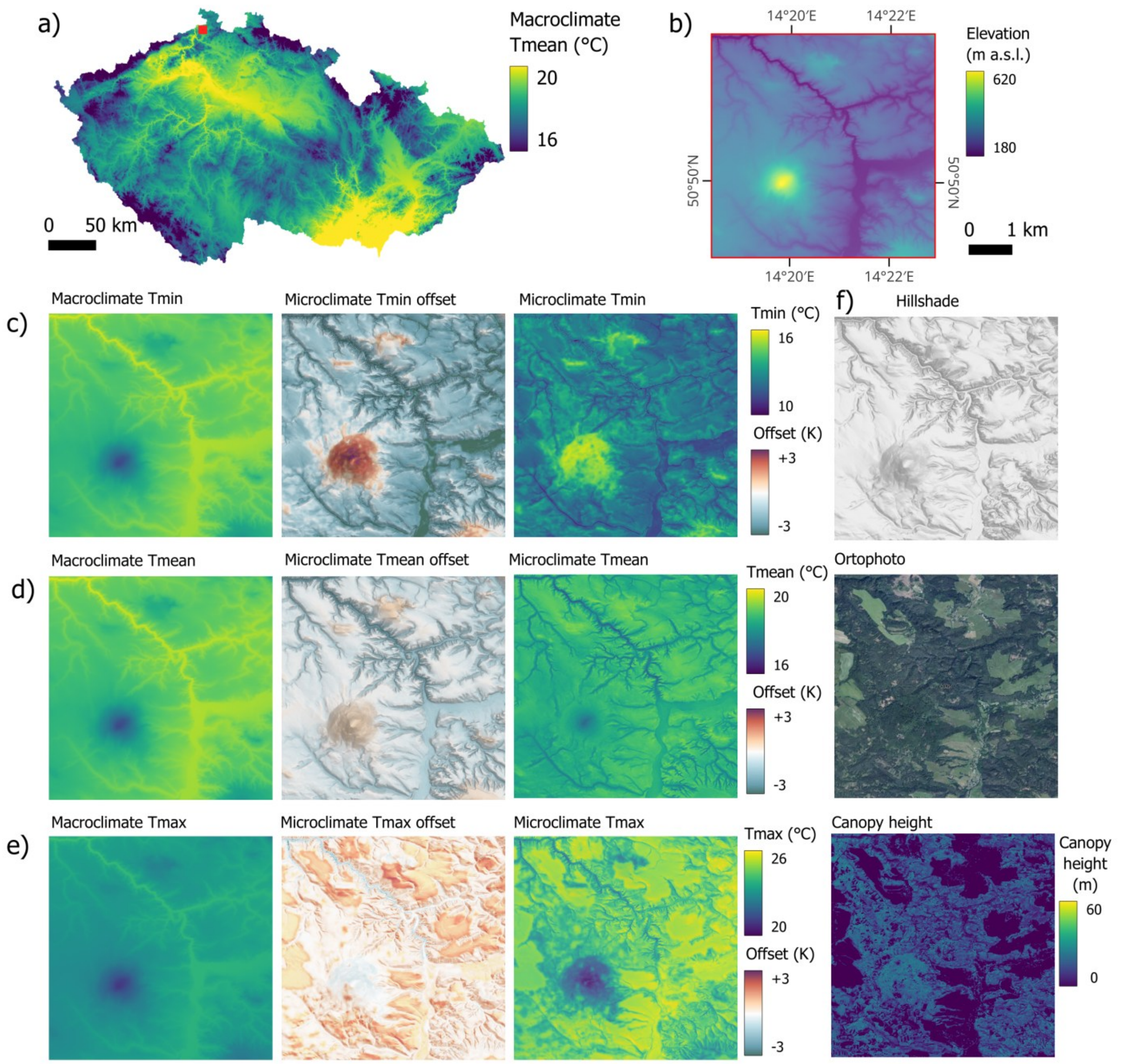

Figure 4 (a) Country-wide map of average daily maximum 2m air temperature in June from ERA5-Land downscaled, elevation-corrected macroclimate data (2018-2024 mean). (b) Example 5 × 5 km area selected for detailed illustration; its location is indicated by the red square in (a). Detailed maps show macroclimate temperature for June (mean; left), microclimatic offsets (middle), and resulting absolute
350 microclimate temperatures for average daily minima (c), means (d), and maxima (e). Topography is illustrated by multidirectional hillshade (f, top), orthophoto (f, middle), and canopy height (f, bottom). Source data: ČÚZK - elevation, orthophoto; Tolan et al., 2024 - Canopy height.

https://doi.org/10.5194/essd-2026-344
Preprint. Discussion started: 19 August 2026

4 Discussion

CzechGrids Micro provides high-resolution maps of microclimate temperature offset with high accuracy for the Czech Republic. This improved performance was enabled by the integration of fine-scale topographic and vegetation predictors with a dense network of microclimatic and weather station observations. Statistical cross-validation (Table 3), range of predicted values (Table 5) and visual inspection of the resulting grids (Figure 4) revealed no obvious artefacts, such as spatial discontinuities or physically implausible values (e.g. minima exceeding maxima), or predictions extrapolated far beyond the observed offset range.

We combined temperature measurements from microclimatic sensors with air temperature data from standard weather stations and found that even measurements from standard weather stations were influenced by local topographic and vegetation effects. This indicates that, despite their standardized placement, weather stations can contribute to modelling local microclimatic variability (Aalto et al., 2017; Meineri and Hylander, 2017). Our results revealed that weather stations were often situated in areas affected by urban heat islands, and in wind-shaded positions at valley bottoms (Figure 2). Thise finding provide important insights into the extend to which local microclimatic conditions influence weather station measurements.

The relatively small partial effect of station type on temperature offsets, which was generally lower than the declared accuracy of the microclimate sensors (0.5°C), suggests that data from properly installed microclimate loggers can be successfully combined with weather station data and that most of the observed variability was explained by selected environmental predictors. After accounting for topographic and vegetation influences, microclimatic stations showed slightly lower minimum temperatures and higher maximum temperatures than weather stations, but these differences were always below 0.5 K. Model uncertainty was similar between weather station data and microclimate station data for minimum and mean temperatures but differed for maximum temperatures, for which the prediction RMSE of microclimate station offsets was 0.48 K higher than for weather station offsets, but still reasonably low (Table 3). This difference was expected because of the simplified radiation shielding used for microclimatic stations (Lundquist and Huggett, 2008; Maclean et al., 2021), the lower accuracy of low-cost microclimatic sensors (Wild et al., 2019), and the substantially greater terrain and vegetation complexity represented by microclimatic stations (Figure 2).

CzechGrids Micro reveals topographic and vegetation effects on microclimate, including cold-air pooling in valleys that affects particularly minimum temperatures and microclimate buffering under forest canopies, particularly influencing maximum temperatures (Figure 4). These effects are strong enough to reverse adiabatic temperature gradients, resulting in local temperature inversions. Consequently, applications relying solely on elevational corrections of macroclimate data can lead to potentially misleading conclusions about the temperature effects on ecological processes and species distributions. Seasonal variation in vegetation-related microclimatic effects reflects differences in phenology of evergreen (conifers) and deciduous (broadleaves and European larch) tree species, and also highlights differences in their microclimate buffering capacity during the growig season.

https://doi.org/10.5194/essd-2026-344
Preprint. Discussion started: 19 August 2026

Interestingly, predicted temperature offsets for daily minima and maxima were not centered around zero but tended to be negative for minima and positive for maxima by -0.88 K and +0.46 K, respectively (Table 5). A plausible explanation for this discrepancy is the difference in temporal resolution between our station measurements (10- and 15-minute) and the hourly ERA5-Land data. Daily temperature extremes may therefore be more accurately captured in the higher-frequency station observations, whereas extremes in the ERA5-Land data may be partially reduced due to temporal smoothing (Johannsen et al., 2019).

To assess this effect, we compared mean daily temperature extremes calculated from raw station time series with the mean extremes from the same data first aggregated to hourly means. Interestingly, hourly aggregation increased daily minima by 0.4 K for 10-minute weather station data and by 0.31 K for 15-minute microclimate data and decreased daily maxima by about 0.28 K for weather station data and 0.14 K for microclimate station data, respectively. However, even when we account for these effects caused by the coarser temporal resolution of the ERA5-Land, the ERA5-Land still substantially underestimates the true diurnal temperature extremes (Table 2). This suggests that diurnal temperature extremes extracted from ERA5-Land should be used with caution. This is especially important in ecological applications, because many ecological processes and species distributions are sensitive to temperature extremes rather than means (Macek et al. 2019).

4.1 General applicability

With the approach outlined in this study, it is possible to produce microclimatic maps at a very fine spatial resolution also in other regions. Nevertheless, the availability of microclimate observations remains a limiting factor in many regions (Lembrechts et al., 2020). Here, we combined standard weather-station observations, which are widely available globally, with microclimate measurements from environments not represented by weather stations. In our study, we achieved an average combined weather/microclimate station density of 0.01 stations km^{-2}, which exceeds the station density used in existing continental- and global-scale products by order of magnitude and has been achieved in only a few regional of country-scale products across the globe (Table 6). Although the physical processes underlying microclimate formation are universal, the magnitude of microclimatic offsets may vary spatially and temporally because of their dependence on local environmental and biological context, atmospheric conditions, and latitude. Therefore, we expect the decrease of the predictive performance in regions with lower microclimate station density. Machine learning methods are increasingly used because of their ability to efficiently handle large datasets and their relatively relaxed assumptions about data structure. However, they can provide unreliable predictions inconsistent with physical laws in data-poor regions and are generally unsuitable for extrapolation beyond the range of the training data (Ludwig et al., 2023; Uxa, 2025), often producing artefacts like discontinuous responses (Figure 5). In contrast, the generalized additive models with used in this study provide smooth responses that become more conservative towards the edges of the observed environmental gradients and are less prone to physically unrealistic response shapes. Many studies have therefore favored simpler linear models or generalized additive models over more flexible machine learning methods for spatial microclimate modelling, particularly when the study area or training dataset is relatively small

(Greiser et al., 2018; Macek et al., 2019; Vandewiele et al., 2023). GAMs may provide a useful compromise between highly flexible, data-driven approaches that are prone to overfitting and linear models that may be overly restrictive when relationships are nonlinear. Their flexibility and computational efficiency make GAMs particularly suitable for generating microclimatic grids at the high spatial and temporal resolutions required for biological and ecological applications while retaining smooth and spatially consistent responses over large areas (Brůna et al., 2026).

The spatial predictor layers used in this study are partly available globally or can be replaced by comparable national products or global datasets at coarser spatial resolutions. Canopy height models are already available globally at sub-meter resolution (Tolan et al., 2024). However, forest cover is dynamic, and microclimatic offsets are therefore expected to change over time as forest canopies develop. In the future, the static canopy height model used to create our dataset should be therefore replaced by annually updated products to generate dynamic offset maps that account for changes in forest structure. Until recently, this was not possible, because reliable, annually resolved, high-resolution and large-scale canopy height models were not available. However, the development of such datasets is an active area of research. A promising candidate for replacing the Tolan et al. (2024) canopy height model is ECHOSAT CHM (Pauls et al., 2026), which currently provides annual canopy height estimates globally for 2018–2024.

Generalizing vegetation effects in global microclimate models may also be challenging because of differences in physiology and phenology of dominant plant species across biomes. In this study, we used an NDVI-based indicator to account for seasonal differences in the effects of deciduous and evergreen tree canopies on understory microclimate. A similar approach could be applied elsewhere because remotely sensed and regularly updated NDVI data are globally available.

Freely available global elevation models (e.g. SRTM, FABDEM, and ASTER) currently provide spatial resolutions of approximately 30 m, which is generally sufficient for microclimate modelling. Nevertheless, for many countries, national digital terrain models based on LiDAR data offer spatial resolutions of 10 m or finer (Bielski et al., 2024), which allows to capture even the very fine-scale effects of land-surface topography. Because topography changes relatively little over time, except in areas affected by active mining, landslides, or other major disturbances, the use of static DTMs is widely appropriate for microclimate offset modelling.

Our model also omitted some microclimatic effects that we considered irrelevant to our study region. Specifically, we did not account for the effects of proximity to the sea, which have been incorporated into previous microclimate models (Haesen et al., 2021; Meineri and Hylander, 2017), because our study region is a landlocked country located far from the coast and these broad-scale effects are incorporated to the ERA5-Land. Nevertheless, such effects may become important when applying the approach to coastal regions or at broader spatial scales and would therefore need to be incorporated into models developed for other regions.

4.2 Comparison to existing products

Available microclimate grids differ in spatial coverage, temporal resolution, and conceptual approaches to model microclimatic processes (Table 6). Compared to microclimate grids with global/continental coverage, CzechGrids Micro provides superior

https://doi.org/10.5194/essd-2026-344
Preprint. Discussion started: 19 August 2026

spatial resolution supported by very high density of *in-situ* observation data for temperature and fine-scale spatial predictors. Low spatial cross-validation RMSE (0.58 K for mean T offsets) and simultaneously high R^2 values demonstrate very good predictive performance of CzechGrids Micro. This performance exceeds typical values reported for global and continental-scale products, including Global Maps of Soil Temperature (RMSE = 2.2 K for monthly mean topsoil temperature; (Lembrechts et al., 2022), ForestTemp (RMSE = 1.19 K for monthly mean T offset; (Haesen et al., 2021), and even comparable national-scale models such as the Swiss microclimatic map based on radiative transfer modelling (RMSE = 1.2 K for mean air temperature at 1 m; (Zellweger et al., 2024). These comparisons should, however, be interpreted cautiously due to differences in modelled vertical layers and geographic extent.

Regional models may achieve even finer spatial resolution and higher accuracy (Table 6). For example, high-resolution microclimatic grids for the Bohemian Forest Ecosystem reported RMSE = 0.42 K for annual mean 2 m air temperature modelled at 5 m spatial resolution (Brůna et al., 2026), mean summer temperature offset grids with 20 m resolution for Berchtesgaden NP reached RMSE of 0.51 K (Vandewiele et al., 2023), while annual mean temperature microclimate grids for Kilpisjärvi region in Sub-Arctic Finland at 3 m spatial resolution reported RMSE of 0.61 K. These models typically rely on dense LiDAR point clouds obtained during leaf-on period for vegetation effects modelling and are trained using a high-density of microclimatic station network (Table 6), which are currently not feasible at national or broader scales. Although high-density, leaf-on LiDAR is currently not available for the entire Czech Republic, its future availability could further improve the accuracy of national-scale microclimate modelling.

For further illustration of differences among microclimatic modelling approaches, we compared our grids with ForestTemp dataset, which has the most comparable spatial and temporal resolution (Figure 5, Figure D1-2). While ForestTemp provides near-surface (15 cm) air temperature offsets only for forests, CzechGrids Micro provides 2 m air temperature offsets for the entire landscape. Although the general patterns appear to be driven by similar environmental factors, ForestTemp shows more localized extremes, particularly for maximum temperatures. This could reflect the inherently higher variability of air temperatures closer to the ground (Geiger et al., 2009) but potentially also modelling artefacts associated with the boosted regression tree approach, causing discontinuous responses, such as those observed on steep slopes (cf. Figure S2 in (Haesen et al., 2021)).

https://doi.org/10.5194/essd-2026-344
Preprint. Discussion started: 19 August 2026

Open Access Earth System Science Data Discussions

480 **Table 6** Characteristics of CzechGrids Micro in comparison with selected high-resolution climatic grids. Grids are ordered by decreasing spatial extent.

Name	Geographic coverage	Description	Layer	Method*	Spatial resolution	Ref. period	N†	Area km^2	Density km^{-2}	Reference
CHELSA-climatologies V2.1	Global	Monthly min, mean, max T climatologies	air 2 m	SDWN	30 arcsec (~1km)	1981-2010	NA	149M	NA	(Karger et al., 2021)
WorldClim 2	Global (land)	Monthly min, mean, max T climatologies	air 2 m	SI	30 arcsec (~1km)	1970-2000	20,268	149M	0.000136	(Fick and Hijmans, 2017)
Global maps of soil temperature	Global (land), without Antarctica	Monthly T offsets & climatologies	soil 0-5 cm soil 5-15 cm	RF	1 km	2000-2020	7,251	134M	0.000054	(Lembrechts et al., 2022)
ForestTemp/ForestClim	European forests	Monthly mean, min, max T offsets / climatologies	air 15 cm	BRT	25 m	2000-2020	1,092/ 1,197	1.96M	0.00055/ 0.00061	(Haesen et al., 2021, 2023a)
CzechGrids Micro	Czechia	Monthly min, mean, max T offsets	air 2 m	GAM	10 m	2018-2024	811	78,866	0.0103	this study
Monthly topsoil and near surface microclimate temperature data for Switzerland	Switzerland	Monthly (April-October) min, mean, max T offsets	air 1 m air 5 cm soil 5 cm	LME	10 m	2021-2022	107	41,248	0.00259	(Zellweger et al., 2024)
Monthly microclimate models in a managed boreal forest landscape	Central Sweden	Monthly temperatures (min, mean, max)	air 5 cm	LR	25 m	2015-2016	203	16,135	0.0126	(Greiser et al., 2018)
High-resolution microclimatic grids for the Bohemian Forest Ecosystem	Šumava NP (CZ), Bavarian Forest NP (DE)	Annual max (95th percentile), mean, min (5th percentile) T	air 2 m air 15 cm soil 8 cm	GAM	5 m	2019-2020	270	930	0.290	(Brůna et al., 2026)
České Středohoří	České Středohoří (CZ)	Growing season (May-September): max (95th percentile), mean, min (5th percentile) T	air 2 m	LR	5 m	2015	46	400	0.115	(Macek et al., 2019)
A Gridded Microclimate Dataset from a Sub-Arctic Biodiversity Hotspot in Finland	Kilpisjärvi (FI)	Monthly min, mean, max T, bioclimatic variables, soil moisture	air 15 cm soil 8 cm	RF	3 m	2019-2023	430	296	0.688	(Niittynen et al., 2024)
Atlas of forest microclimate in the national parks Bohemian and Saxon Switzerland, version 1.0	Bohemian Switzerland NP (CZ), Saxon Switzerland NP (DE)	Annual max (95th percentile), mean, min (5th percentile) T	air 2 m air 15 cm soil 8 cm	GAM	5 m	2018 - 2021	219	173	1.27	(Man et al., 2022a)
Mapping spatial microclimate patterns in mountain forests from LiDAR	Berchtesgaden NP (DE) (forests)	Summer (July-August) min, mean, max T offsets	air 15 cm	LR	20 m	2021	150	86	1.74	Vandewiele et al. 2023

**Abbreviations:* SDWN = *Statistical Downscaling, SI = Spatial Interpolation, ML = Machine Learning, RF = Random Forest, BRT = Boosted Regression Trees, GAM = Generalized Additive Models, LME = Linear Mixed Effect model, LR = Linear Regression.*

†N is the number of unique localities used for model training/interpolation.

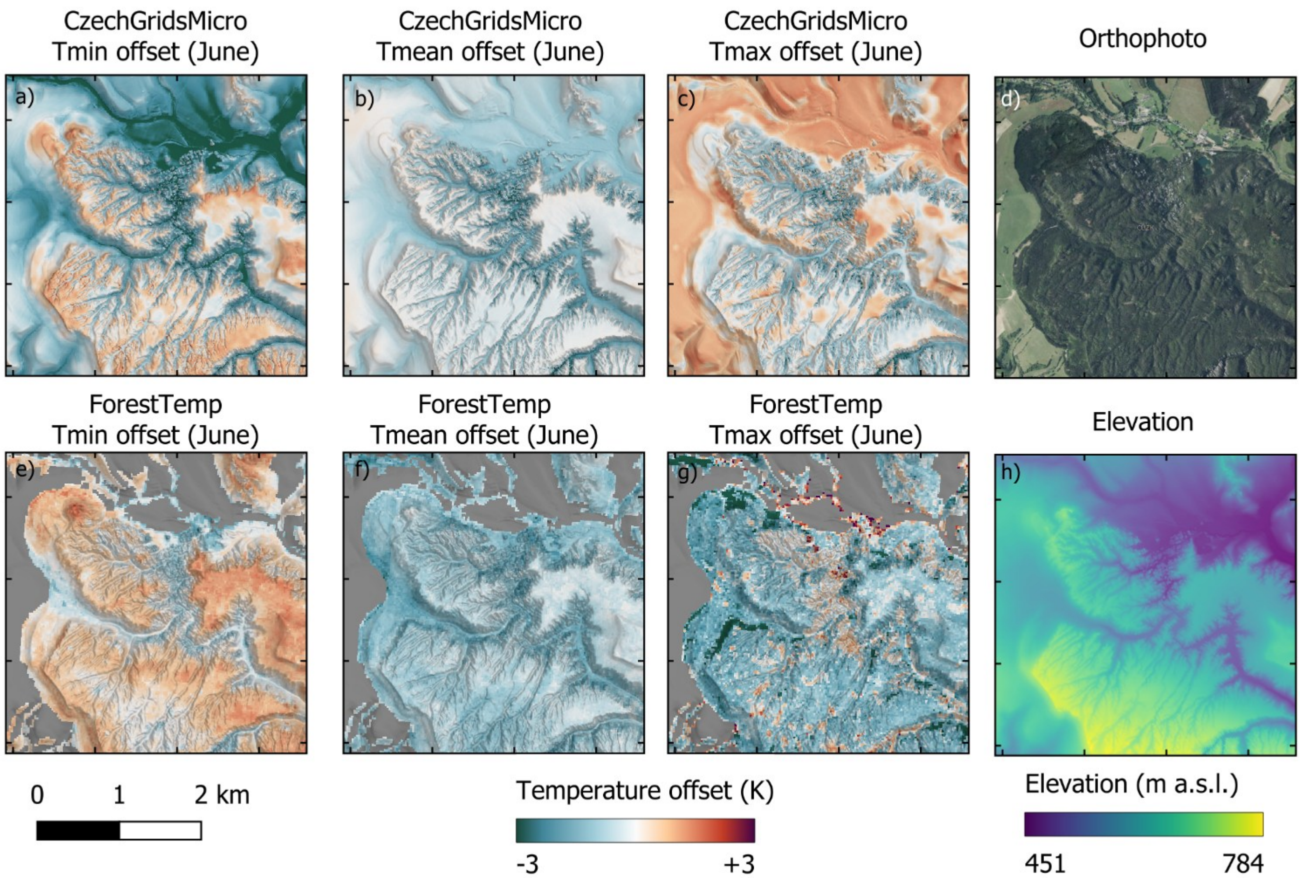

Figure 5 Comparison of microclimatic offsets for 2 m air temperature from CzechGrids Micro (a – c; this study) and for 15 cm air temperature from ForestTemp (e – g; Haesen et al., 2021). Offset maps are overlayed over shaded relief. Orthophoto (d) and elevation (h) are showed for reference. Note that offsets in ForestTemp are available only for forest stands. Data sources: ČÚZK (orthophoto, elevation).

4.3 Usage guidelines

The provided grids represent expected monthly microclimatic temperature offsets relative to elevation-corrected macroclimate, reflecting vegetation conditions around 2019-2021. Absolute microclimatic temperatures can be obtained by adding the offsets to independently downscaled ERA5-Land temperatures (elevation corrected) for the period of interest. However, uncertainty in the resulting grids increases with temporal distance from the vegetation reference period due to increasing discrepancy between actual vegetation structure and vegetation structure used in offset prediction. Application with alternative climate datasets requires consistent downscaling and may introduce systematic biases. CzechGrids Micro are primarily intended for use in ecological applications, e.g. in species distribution modelling, for identification of potential microclimatic refugia, or planning in forestry and nature conservation. However, the range of potential applications is much wider.

https://doi.org/10.5194/essd-2026-344
Preprint. Discussion started: 19 August 2026

Code, data, or code and data availability

The CzechGrids Micro monthly temperature offset grids and supporting code and data are available at the Zenodo repository at https://doi.org/10.5281/zenodo.18472086 (Macek et al., 2026) under CC-BY-4.0 license.

Conclusion

The CzechGrids Micro dataset provides monthly and annual microclimate temperature offset grids for the Czech Republic at 10 m spatial resolution based on generalized additive models trained on nearly 49,000 monthly observations from 810 localities. The dataset includes separate grids for daily minimum, mean, and maximum air temperature offsets and captures topographic, urban heat island, and vegetation effects on local climate. Spatial cross-validation showed very good predictive performance, with RMSE values between 0.58 K and 1.01 K and R^2 between 0.71 and 0.82. Compared to macroclimate alone, the grids substantially improve representation of near-surface thermal heterogeneity and provide a detailed basis for ecological research, biodiversity modelling, and climate-change impact assessments at fine spatial scales.

https://doi.org/10.5194/essd-2026-344
Preprint. Discussion started: 19 August 2026

Appendix A: Vegetation characteristics processing

This appendix provides details about the workflow used for processing vegetation characteristics predictors, including canopy height, tree cover, and evergreen cover layers derived from remote sensing data.

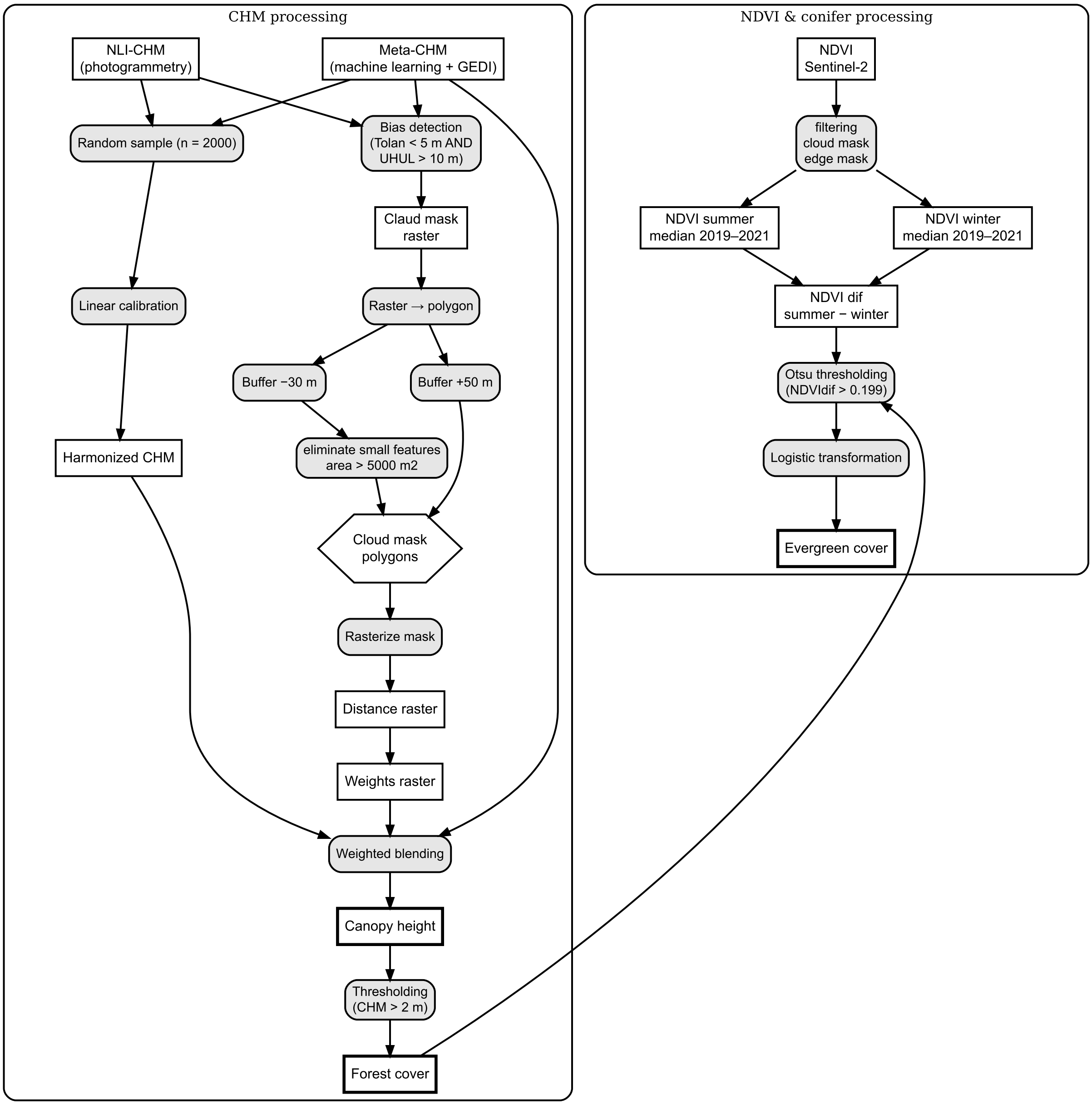

515 **Figure A1** Workflow diagram for vegetation indices processing. Raster layers are indicated by rectangular boxes, processing steps by rounded boxes and hexagonal boxes represent polygon layers. Left box illustrates creation of gap-filled Canopy height grids from Meta–WRI Global Canopy Height Model (Meta-CHM, Tolan et al. 2024) and national photogrammetry canopy height model (NLI-CHM, Czech Forestry Institute, https://nli.gov.cz). Right box illustrates creation of evergreen cover grids from normalized Sentinel-2 NDVI products. For threshold value estimation using Otsu algorithm, only forest pixels were used. Evergreen cover for non-forest pixels was set to zero.

https://doi.org/10.5194/essd-2026-344
Preprint. Discussion started: 19 August 2026

Appendix B: Empirical lapse rates

This appendix provides summary of empirical temperature lapse rates derived from ERA5-Land data and used for downscaling macroclimatic temperatures to the 10 m spatial resolution of CzechGrids Micro.

Table B1 Monthly temperature lapse rates (°C·km⁻¹) calculated from ERA5-Land daily mean (T_{MEAN}), minimum (T_{MIN}) and maximum (T_{MAX}) air temperatures. Values represent average monthly lapse rates over 2018-2024, together with minimum and maximum values observed over this period.

Month	T_{MIN}			T_{MEAN}			T_{MAX}		
	average	min	max	average	min	max	average	min	max
1	-5.45	-6.91	-3.59	-5.43	-6.71	-3.53	-5.62	-6.54	-3.45
2	-5.58	-7.30	-3.26	-6.04	-7.04	-4.00	-6.86	-8.13	-5.06
3	-4.66	-5.30	-3.39	-5.82	-6.80	-5.17	-6.85	-7.89	-6.01
4	-5.17	-5.94	-4.17	-6.11	-6.58	-5.74	-6.84	-7.35	-6.10
5	-5.44	-5.76	-5.31	-6.18	-6.52	-5.62	-6.82	-7.51	-5.99
6	-5.40	-6.19	-5.08	-6.25	-6.98	-5.86	-6.96	-7.93	-6.38
7	-5.69	-6.08	-5.06	-6.85	-7.41	-6.31	-7.82	-8.64	-7.30
8	-5.45	-6.18	-4.76	-6.52	-7.47	-5.61	-7.44	-8.58	-6.23
9	-4.81	-5.43	-4.38	-5.81	-6.28	-5.42	-6.77	-7.04	-6.44
10	-4.64	-5.04	-4.16	-5.17	-5.89	-4.30	-5.63	-6.79	-4.40
11	-4.33	-5.48	-3.76	-4.67	-5.96	-3.92	-4.78	-6.42	-3.39
12	-4.68	-5.78	-4.02	-4.74	-5.47	-4.20	-4.88	-5.66	-4.15
1-12	**-5.11**	**-7.30**	**-3.26**	**-5.80**	**-7.47**	**-3.53**	**-6.44**	**-8.64**	**-3.39**

https://doi.org/10.5194/essd-2026-344
Preprint. Discussion started: 19 August 2026

Open Access Earth System Science Data Discussions

Appendix C: Partial effects

This appendix presents partial effects of predictors included in the generalized additive models for monthly minimum (Figure C1), mean (Figure C2), and maximum (Figure C3) microclimate temperature offsets, illustrating the shape and seasonal variation of individual responses.

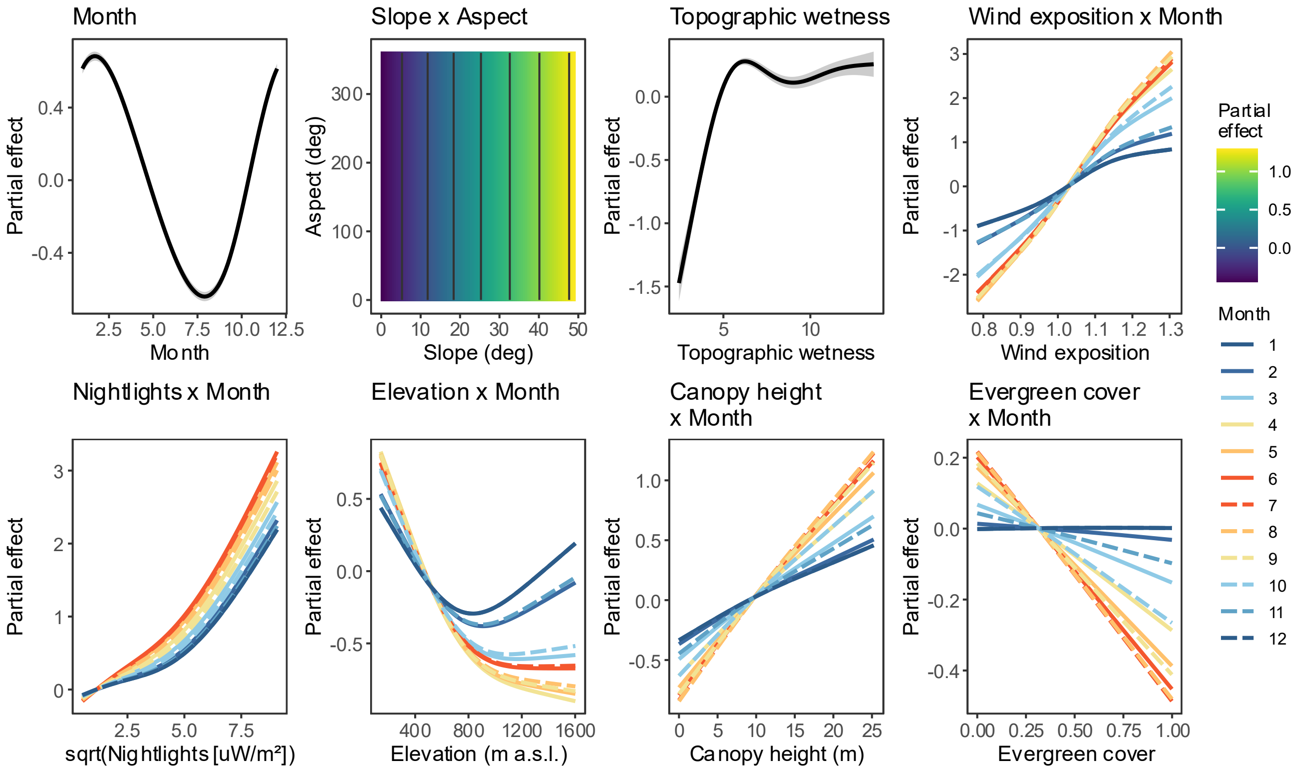

Figure C1 Partial effects for T_{MIN} offsets. For predictors exhibiting significant interactions with month, effects are presented as the sum of the main effect and the interaction term, with separate curves shown for each month. For predictors without significant interactions, only the main effect is displayed, together with the 95% confidence interval. Isolines for the slope × aspect interaction raster are plotted at 0.25 K intervals.

https://doi.org/10.5194/essd-2026-344
Preprint. Discussion started: 19 August 2026

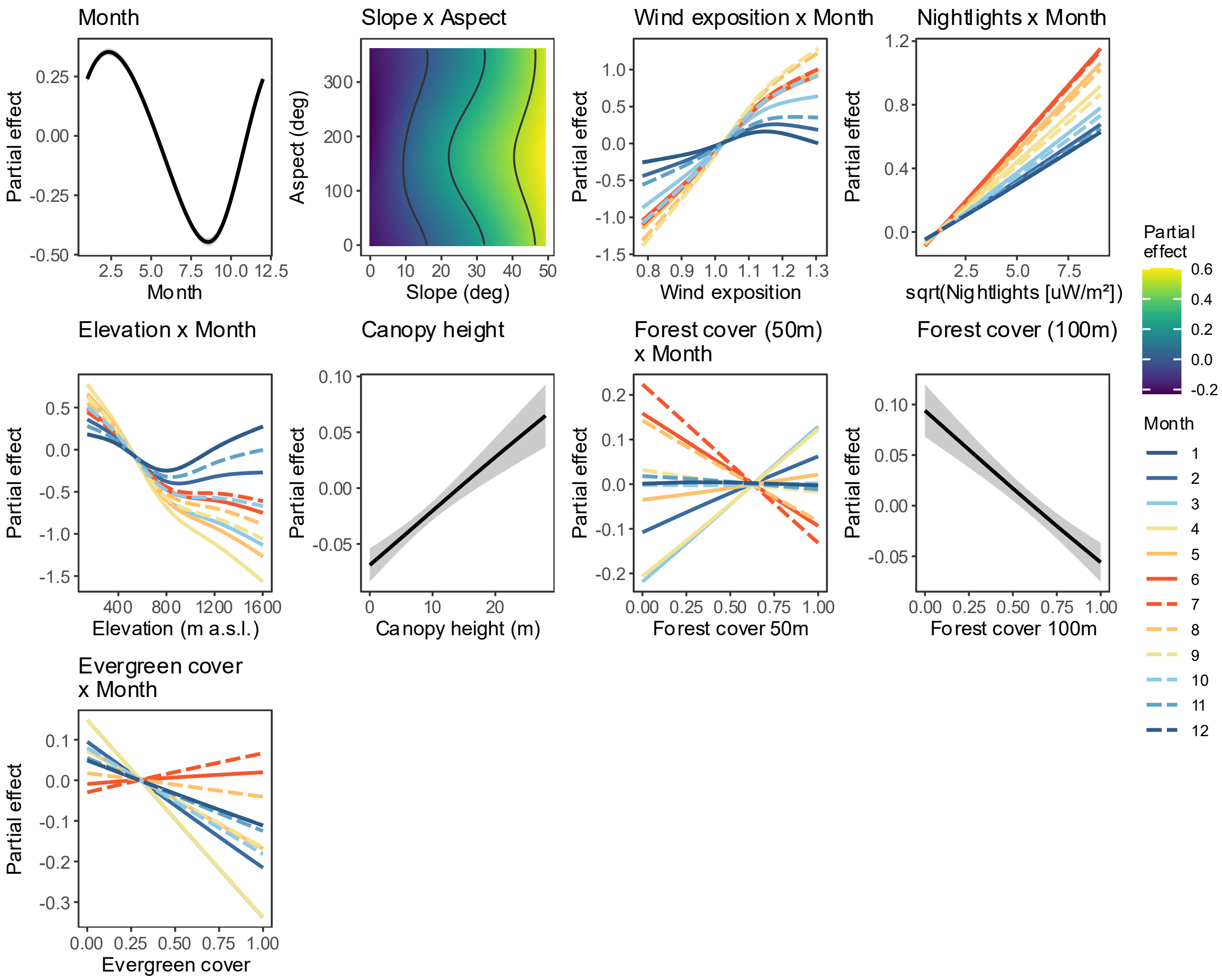

Figure C2 Partial effects for T_{MEAN} offsets. For predictors exhibiting significant interactions with month, effects are presented as the sum of the main effect and the interaction term, with separate curves shown for each month. For predictors without significant interactions, only the main effect is displayed, together with the 95% confidence interval. Isolines for the slope × aspect interaction are plotted at 0.25 K intervals.

https://doi.org/10.5194/essd-2026-344
Preprint. Discussion started: 19 August 2026

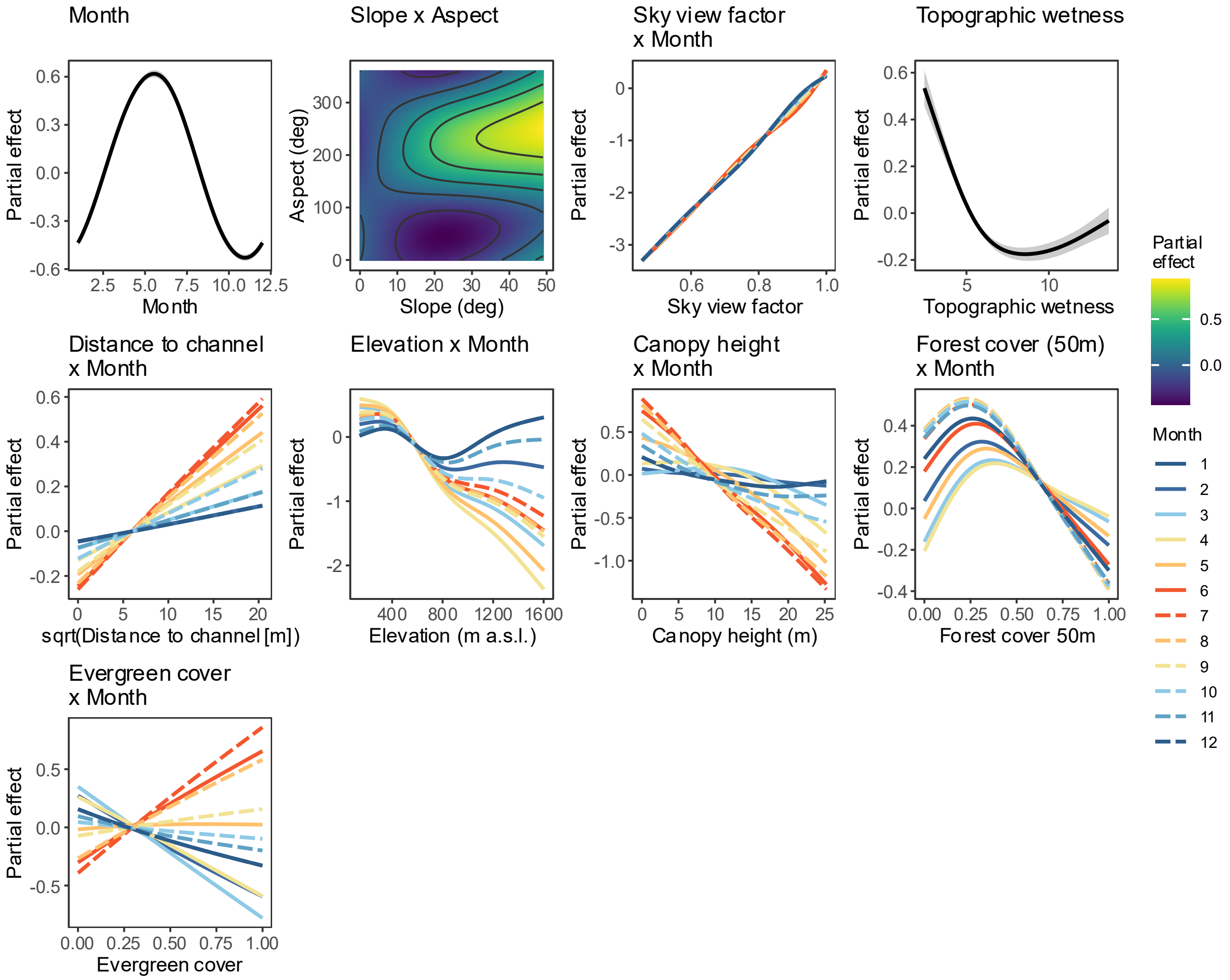

Figure C3 Partial effects for T_{MAX} offsets. For predictors exhibiting significant interactions with month, effects are presented as the sum of the main effect and the interaction term, with separate curves shown for each month. For predictors without significant interactions, only the main effect is displayed, together with the 95% confidence interval. Isolines for the slope × aspect interaction raster are plotted at 0.25 K intervals.

https://doi.org/10.5194/essd-2026-344
Preprint. Discussion started: 19 August 2026

Open Access Earth System Science Data Discussions

Appendix D: Comparison with ForestTemp microclimate offsets

This appendix presents a detailed comparison between CzechGrids Micro and the ForestTemp dataset, illustrating similarities and differences in predicted spatial patterns of microclimate temperature offsets within the overlapping study area.

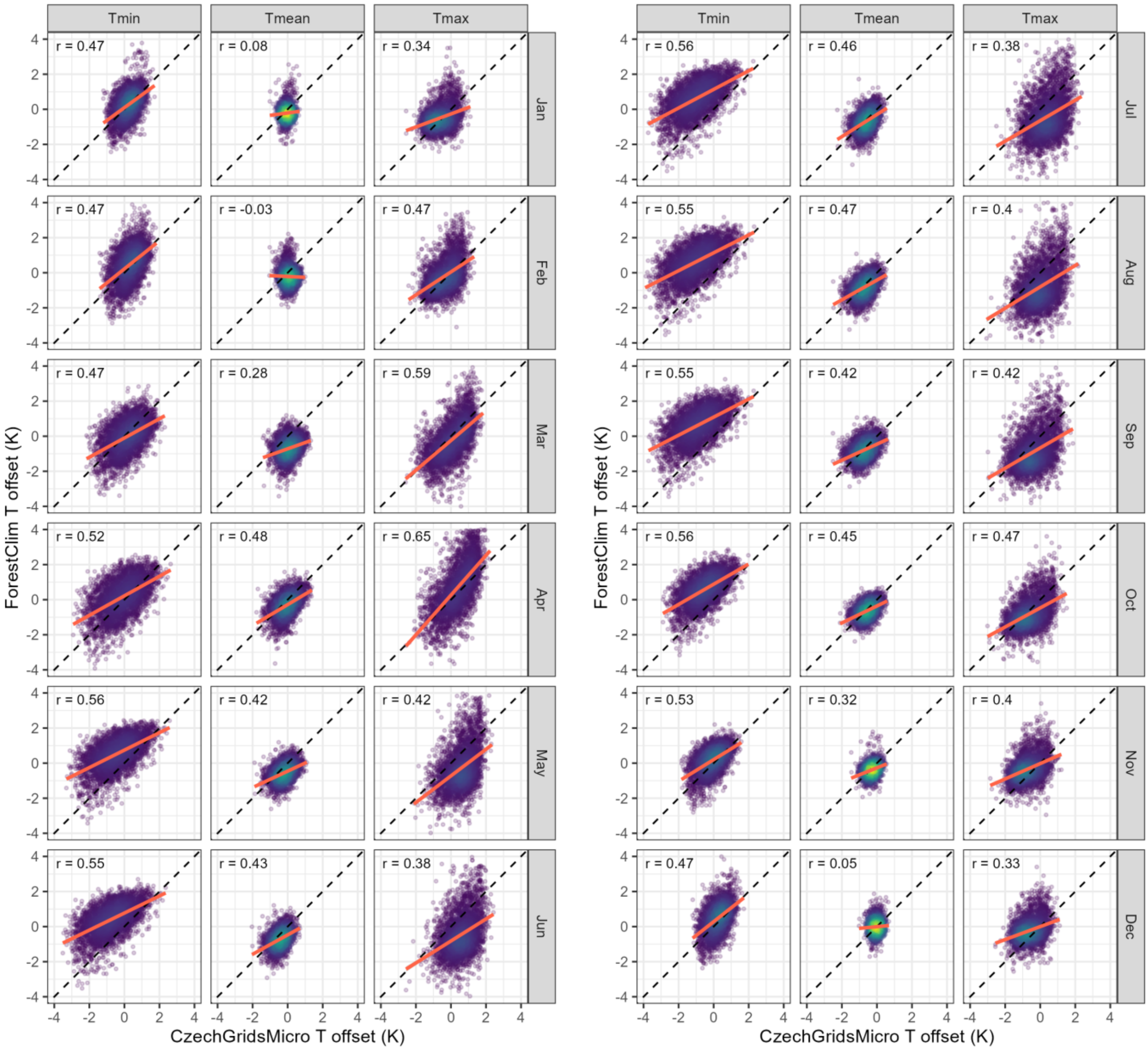

Figure D1 – Pairwise correlations between offsets from CzechGrids Micro and ForestTemp (Tmean) / ForestClim (Tmin, Tmax). Columns are defined by monthly offset variable (minimum, mean, maximum) and rows by months of the year. Correlation coefficient (r) is indicated in each panel. Note that CzechGrids Micro and ForestTemp offsets represents different air layer (2 m vs. 15cm). Values are based on random sample of 3,799 point locations with complete pairwise observations.

https://doi.org/10.5194/essd-2026-344
Preprint. Discussion started: 19 August 2026

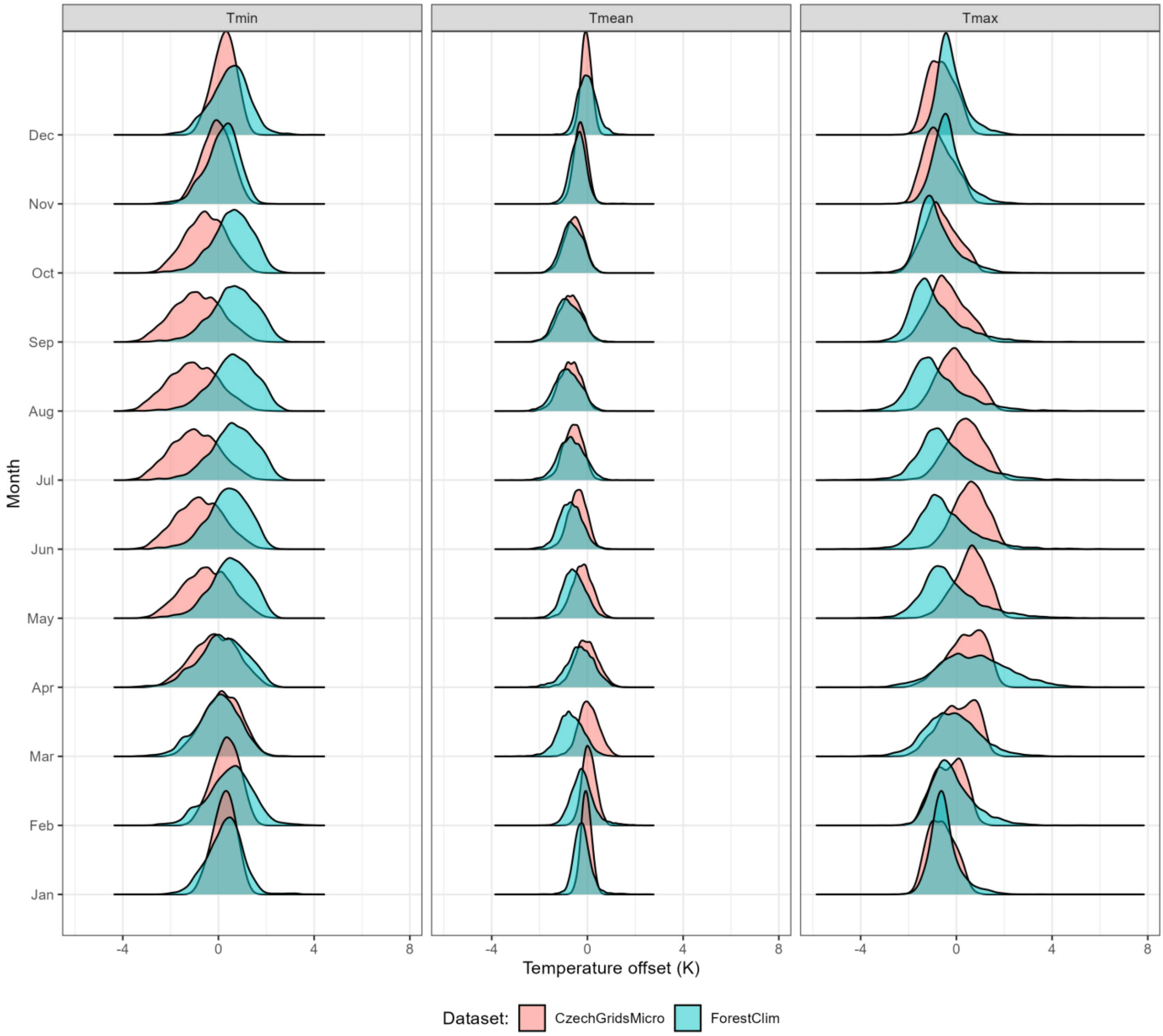

565 **Figure D2** Ridgeplots showing density distribution of temperature offsets for individual months from CzechGrids Micro (pink) and ForestTemp (Tmean) / ForestClim (Tmin, Tmax) (aqua). Values are based on random sample of 3,799 point locations with complete pairwise observations. Note that these datasets differ in reference macroclimate grids and vertical layer (2 m vs. 15 cm).

https://doi.org/10.5194/essd-2026-344
Preprint. Discussion started: 19 August 2026

Author contributions

Conceptualization: M. Macek, M.Man, JB, JW, and MK. Data curation: TK, LH, AR, M. Macek, M. Man. Model development, spatial predictions: M. Man and M. Macek. Data processing: M. Man, M. Macek (R, SAGA GIS), JP (Google Earth Engine). MK, JW, JB & M. Man funding acquisition. All authors participated data acquisition, manuscript writing and editing. M. Macek lead the writing.

Competing interests

Authors declare no competing interests.

Acknowledgements

We thank all colleagues who participated in field data collection. We thank the Nature Conservation Agency of the Czech Republic, the administrations of the Šumava NP, Bohemian Switzerland NP, Bohemian Karst PLA, and České Středohoří PLA; as well as the Czech State Forest and private forest owners for granting permission to conduct the research and their administrative and logistical support. We thank the Czech Hydrometeorological Institute for providing weather station data and the 'Blue Cat Research Team' from the Department of Forest Ecology, Landscape Research Institute in Brno for providing microclimate data. We also acknowledge the Metacentrum CESNET e-Infrastruktura CZ (e-INFRA LM2018140) for providing resources for the processing of large topographic grids. AI tools (ChatGPT by OpenAI) were used to assist language editing and to aid coding in R.

Financial support

This research was supported by the Czech Academy of Sciences (RVO 67985939). National-level network in managed forests was maintained with support from the Czech Science Foundation (GACR 23-06614S). National-level network in protected forests received support from the Technology Agency of the Czech Republic (SS02030018). Microclimate network in the Bohemian Forest NP was maintained with the support from the Technology Agency of the Czech Republic (SS06010011).

References

Aalto, J., Riihimäki, H., Meineri, E., Hylander, K., and Luoto, M.: Revealing topoclimatic heterogeneity using meteorological station data, International Journal of Climatology, 37, 544–556, https://doi.org/10.1002/joc.5020, 2017.

https://doi.org/10.5194/essd-2026-344
Preprint. Discussion started: 19 August 2026

Ackerly, D. D., Kling, M. M., Clark, M. L., Papper, P., Oldfather, M. F., Flint, A. L., and Flint, L. E.: Topoclimates, refugia, and biotic responses to climate change, Frontiers in Ecology and the Environment, 18, 288–297, https://doi.org/10.1002/fee.2204, 2020.

Ashcroft, M. B.: A method for improving landscape scale temperature predictions and the implications for vegetation modelling, Ecological Modelling, 197, 394–404, 2006.

Ashcroft, M. B.: Identifying refugia from climate change, Journal of Biogeography, 9999, 2010.

Beck, H. E., Zimmermann, N. E., McVicar, T. R., Vergopolan, N., Berg, A., and Wood, E. F.: Present and future köppen-geiger climate classification maps at 1-km resolution, Scientific Data, 5, 1–12, https://doi.org/10.1038/sdata.2018.214, 2018.

Bielski, C., López-Vázquez, C., Grohmann, C. H., Guth, P. L., Hawker, L., Gesch, D., Trevisani, S., Herrera-Cruz, V., Riazanoff, S., Corseaux, A., Reuter, H. I., and Strobl, P.: Novel Approach for Ranking DEMs: Copernicus DEM Improves One Arc Second Open Global Topography, IEEE Transactions on Geoscience and Remote Sensing, 62, 1–22, https://doi.org/10.1109/TGRS.2024.3368015, 2024.

Böhner, J. and Antonić, O.: Land-surface parameters specific to topo-climatology, in: Geomorphometry: concepts, software, applications, vol. 33, edited by: Hengl, T. and Reuter, H. U., Elsevier, Amsterdam, 195–226, https://doi.org/10.1016/S0166-2481(08)00008-1, 2009.

Brůna, J., Macek, M., Man, M., Hederová, L., Klinerová, T., Moudrý, V., Heurich, M., Červenka, J., Wild, J., and Kopecký, M.: High-resolution microclimatic grids for the Bohemian Forest Ecosystem based on in situ measurements, Scientific Data, https://doi.org/10.1038/s41597-026-06566-z, 2026.

Conrad, O., Bechtel, B., Bock, M., Dietrich, H., Fischer, E., Gerlitz, L., Wehberg, J., Wichmann, V., and Böhner, J.: System for Automated Geoscientific Analyses (SAGA) v. 2.1.4, Geoscientific Model Development, 8, 1991–2007, https://doi.org/10.5194/gmd-8-1991-2015, 2015.

Crhová, L., Kliegrová, S., Lipina, P., Tolasz, R., and Valeriánová, A.: Klimatologická ročenka České republiky 2021, Český hydrometeorologický ústav, Praha, 2022.

De Frenne, P., Rodriguez-Sanchez, F., Coomes, D. A., Baeten, L., Verstraeten, G., Vellend, M., Bernhardt-Romermann, M., Brown, C. D., Brunet, J., Cornelis, J., Decocq, G. M., Dierschke, H., Eriksson, O., Gilliam, F. S., Hedl, R., Heinken, T., Hermy, M., Hommel, P., Jenkins, M. a, Kelly, D. L., Kirby, K. J., Mitchell, F. J. G., Naaf, T., Newman, M., Peterken, G., Petrik, P., Schultz, J., Sonnier, G., Van Calster, H., Waller, D. M., Walther, G.-R., White, P. S., Woods, K. D., Wulf, M., Graae, B. J., and Verheyen, K.: Microclimate moderates plant responses to macroclimate warming, Proceedings of the National Academy of Sciences, 110, 18561–18565, https://doi.org/10.1073/pnas.1311190110, 2013.

De Frenne, P., Lenoir, J., Luoto, M., Scheffers, B. R., Zellweger, F., Aalto, J., Ashcroft, M. B., Christiansen, D. M., Decocq, G., De Pauw, K., Govaert, S., Greiser, C., Gril, E., Hampe, A., Jucker, T., Klinges, D. H., Koelemeijer, I. A., Lembrechts, J. J., Marrec, R., Meeussen, C., Ogée, J., Tyystjärvi, V., Vangansbeke, P., and Hylander, K.: Forest microclimates and climate change: Importance, drivers and future research agenda, Global Change Biology, 27, 2279–2297, https://doi.org/10.1111/gcb.15569, 2021.

Ehbrecht, M., Schall, P., Ammer, C., Fischer, M., and Seidel, D.: Effects of structural heterogeneity on the diurnal temperature range in temperate forest ecosystems, Forest Ecology and Management, 432, 860–867, https://doi.org/10.1016/j.foreco.2018.10.008, 2019.

https://doi.org/10.5194/essd-2026-344
Preprint. Discussion started: 19 August 2026

Elvidge, C. D., Zhizhin, M., Ghosh, T., Hsu, F., and Taneja, J.: Annual Time Series of Global VIIRS Nighttime Lights Derived from Monthly Averages : 2012 to 2019, 2021.

Fick, S. E. and Hijmans, R. J.: WorldClim 2: new 1-km spatial resolution climate surfaces for global land areas, International Journal of Climatology, 37, 4302–4315, https://doi.org/10.1002/joc.5086, 2017.

Frey, S. J. K., Hadley, A. S., Johnson, S. L., Schulze, M., Jones, J. A., and Betts, M. G.: Spatial models reveal the microclimatic buffering capacity of old-growth forests, Science Advances, 2, e1501392–e1501392, https://doi.org/10.1126/sciadv.1501392, 2016.

Geiger, R., Aron, R., and Todhunter, P.: The climate near the ground, 7th ed., Rowman & Littlefield, 642 pp., 2009.

Gorelick, N., Hancher, M., Dixon, M., Ilyushchenko, S., Thau, D., and Moore, R.: Google Earth Engine: Planetary-scale geospatial analysis for everyone, Remote Sensing of Environment, 202, 18–27, https://doi.org/10.1016/j.rse.2017.06.031, 2017.

Greiser, C., Meineri, E., Luoto, M., Ehrlén, J., and Hylander, K.: Monthly microclimate models in a managed boreal forest landscape, Agricultural and Forest Meteorology, 250–251, 147–158, https://doi.org/10.1016/j.agrformet.2017.12.252, 2018.

Greiser, C., Hederová, L., Vico, G., Wild, J., Macek, M., and Kopecký, M.: Higher soil moisture increases microclimate temperature buffering in temperate broadleaf forests, Agricultural and Forest Meteorology, 345, 109828, https://doi.org/10.1016/j.agrformet.2023.109828, 2024.

Haesen, S., Lembrechts, J. J., De Frenne, P., Lenoir, J., Aalto, J., Ashcroft, M. B., Kopecký, M., Luoto, M., Maclean, I., Nijs, I., Niittynen, P., Hoogen, J., Arriga, N., Brůna, J., Buchmann, N., Čiliak, M., Collalti, A., De Lombaerde, E., Descombes, P., Gharun, M., Goded, I., Govaert, S., Greiser, C., Grelle, A., Gruening, C., Hederová, L., Hylander, K., Kreyling, J., Kruijt, B., Macek, M., Máliš, F., Man, M., Manca, G., Matula, R., Meeussen, C., Merinero, S., Minerbi, S., Montagnani, L., Muffler, L., Ogaya, R., Penuelas, J., Plichta, R., Portillo-Estrada, M., Schmeddes, J., Shekhar, A., Spicher, F., Ujházyová, M., Vangansbeke, P., Weigel, R., Wild, J., Zellweger, F., and Van Meerbeek, K.: ForestTemp – Sub-canopy microclimate temperatures of European forests, Global Change Biology, 27, 6307–6319, https://doi.org/10.1111/gcb.15892, 2021.

Haesen, S., Lembrechts, J. J., De Frenne, P., Lenoir, J., Aalto, J., Ashcroft, M. B., Kopecký, M., Luoto, M., Maclean, I., Nijs, I., Niittynen, P., van den Hoogen, J., Arriga, N., Brůna, J., Buchmann, N., Čiliak, M., Collalti, A., De Lombaerde, E., Descombes, P., Gharun, M., Goded, I., Govaert, S., Greiser, C., Grelle, A., Gruening, C., Hederová, L., Hylander, K., Kreyling, J., Kruijt, B., Macek, M., Máliš, F., Man, M., Manca, G., Matula, R., Meeussen, C., Merinero, S., Minerbi, S., Montagnani, L., Muffler, L., Ogaya, R., Penuelas, J., Plichta, R., Portillo-Estrada, M., Schmeddes, J., Shekhar, A., Spicher, F., Ujházyová, M., Vangansbeke, P., Weigel, R., Wild, J., Zellweger, F., and Van Meerbeek, K.: <scp>ForestClim</scp> —Bioclimatic variables for microclimate temperatures of European forests, Global Change Biology, 29, 2886–2892, https://doi.org/10.1111/gcb.16678, 2023a.

Haesen, S., Lenoir, J., Gril, E., De Frenne, P., Lembrechts, J. J., Kopecký, M., Macek, M., Man, M., Wild, J., and Van Meerbeek, K.: Microclimate reveals the true thermal niche of forest plant species, Ecology Letters, 1–13, https://doi.org/10.1111/ele.14312, 2023b.

Hijmans, R. J.: terra: Spatial Data Analysis, , https://doi.org/10.32614/CRAN.package.terra, 2026.

Johannsen, F., Ermida, S., Martins, J. P. A., Trigo, I. F., Nogueira, M., and Dutra, E.: Cold bias of ERA5 summertime daily maximum land surface temperature over Iberian Peninsula, Remote Sensing, 11, https://doi.org/10.3390/rs11212570, 2019.

https://doi.org/10.5194/essd-2026-344
Preprint. Discussion started: 19 August 2026

Jucker, T., Hardwick, S. R., Both, S., Elias, D. M. O., Ewers, R. M., Milodowski, D. T., Swinfield, T., and Coomes, D. A.: Canopy structure and topography jointly constrain the microclimate of human-modified tropical landscapes, Global Change Biology, 24, 5243–5258, https://doi.org/10.1111/gcb.14415, 2018.

Karger, D. N., Conrad, O., Böhner, J., Kawohl, T., Kreft, H., Soria-Auza, R. W., Zimmermann, N. E., Linder, P. H., and Kessler, M.: Climatologies at high resolution for the earth's land surface areas, , https://doi.org/https://www.doi.org/10.16904/envidat.228., 2021.

Klinges, D. H., Baecher, J. A., Lembrechts, J. J., Maclean, I. M. D., Lenoir, J., Greiser, C., Ashcroft, M., Evans, L. J., Kearney, M. R., Aalto, J., Barrio, I. C., De Frenne, P., Guillemot, J., Hylander, K., Jucker, T., Kopecký, M., Luoto, M., Macek, M., Nijs, I., Urban, J., van den Brink, L., Vangansbeke, P., Von Oppen, J., Wild, J., Boike, J., Canessa, R., Nosetto, M., Rubtsov, A., Sallo-Bravo, J., and Scheffers, B. R.: Proximal microclimate: Moving beyond spatiotemporal resolution improves ecological predictions, Global Ecology and Biogeography, 33, e13884, https://doi.org/10.1111/geb.13884, 2024.

Kopecký, M., Macek, M., and Wild, J.: Topographic Wetness Index calculation guidelines based on measured soil moisture and plant species composition, Science of The Total Environment, 757, 143785, https://doi.org/10.1016/j.scitotenv.2020.143785, 2021.

Kopecký, M., Hederová, L., Macek, M., Klinerová, T., and Wild, J.: Forest plant indicator values for moisture reflect atmospheric vapour pressure deficit rather than soil water content, New Phytologist, 244, 1801–1811, https://doi.org/10.1111/nph.20068, 2024.

Landini, G., Randell, D. A., Fouad, S., and Galton, A.: Automatic thresholding from the gradients of region boundaries, Journal of Microscopy, 265, 185–195, https://doi.org/https://doi.org/10.1111/jmi.12474, 2017.

Lembrechts, J. J., Nijs, I., and Lenoir, J.: Incorporating microclimate into species distribution models, Ecography, 42, 1267–1279, https://doi.org/10.1111/ecog.03947, 2019.

Lembrechts, J. J., Aalto, J., Ashcroft, M. B., De Frenne, P., Kopecký, M., Lenoir, J., Luoto, M., Maclean, I. M. D., Roupsard, O., Fuentes-Lillo, E., García, R. A., Pellissier, L., Pitteloud, C., Alatalo, J. M., Smith, S. W., Björk, R. G., Muffler, L., Ratier Backes, A., Cesarz, S., Gottschall, F., Okello, J., Urban, J., Plichta, R., Svátek, M., Phartyal, S. S., Wipf, S., Eisenhauer, N., Puşcaş, M., Turtureanu, P. D., Varlagin, A., Dimarco, R. D., Jump, A. S., Randall, K., Dorrepaal, E., Larson, K., Walz, J., Vitale, L., Svoboda, M., Finger Higgens, R., Halbritter, A. H., Curasi, S. R., Klupar, I., Koontz, A., Pearse, W. D., Simpson, E., Stemkovski, M., Jessen Graae, B., Vedel Sørensen, M., Høye, T. T., Fernández Calzado, M. R., Lorite, J., Carbognani, M., Tomaselli, M., Forte, T. G. W., Petraglia, A., Haesen, S., Somers, B., Van Meerbeek, K., Björkman, M. P., Hylander, K., Merinero, S., Gharun, M., Buchmann, N., Dolezal, J., Matula, R., Thomas, A. D., Bailey, J. J., Ghosn, D., Kazakis, G., de Pablo, M. A., Kemppinen, J., Niittynen, P., Rew, L., Seipel, T., Larson, C., Speed, J. D. M., Ardö, J., Cannone, N., Guglielmin, M., Malfasi, F., Bader, M. Y., Canessa, R., Stanisci, A., Kreyling, J., Schmeddes, J., Teuber, L., Aschero, V., Čiliak, M., Máliš, F., De Smedt, P., Govaert, S., Meeussen, C., Vangansbeke, P., Gigauri, K., Lamprecht, A., Pauli, H., Steinbauer, K., Winkler, M., Ueyama, M., et al.: SoilTemp: A global database of near-surface temperature, Global Change Biology, 6616–6629, https://doi.org/10.1111/gcb.15123, 2020.

Lembrechts, J. J., van den Hoogen, J., Aalto, J., Ashcroft, M. B., De Frenne, P., Kemppinen, J., Kopecký, M., Luoto, M., Maclean, I. M. D., Crowther, T. W., Bailey, J. J., Haesen, S., Klinges, D. H., Niittynen, P., Scheffers, B. R., Van Meerbeek, K., Aartsma, P., Abdalaze, O., Abedi, M., Aerts, R., Ahmadian, N., Ahrends, A., Alatalo, J. M., Alexander, J. M., Allonsius, C. N., Altman, J., Ammann, C., Andres, C., Andrews, C., Ardö, J., Arriga, N., Arzac, A., Aschero, V., Assis, R. L., Assmann, J. J., Bader, M. Y., Bahalkeh, K., Barančok, P., Barrio, I. C., Barros, A., Barthel, M., Basham, E. W., Bauters, M., Bazzichetto, M., Marchesini, L. B., Bell, M. C., Benavides, J. C., Benito Alonso, J. L., Berauer, B. J., Bjerke, J. W., Björk, R. G., Björkman, M. P., Björnsdóttir, K., Blonder, B., Boeckx, P., Boike, J., Bokhorst, S., Brum, B. N. S., Brůna, J., Buchmann, N., Buysse, P., Camargo, J. L., Campoe, O. C., Candan, O., Canessa, R., Cannone, N., Carbognani, M., Carnicer, J., Casanova-Katny, A.,

https://doi.org/10.5194/essd-2026-344
Preprint. Discussion started: 19 August 2026

Cesarz, S., Chojnicki, B., Choler, P., Chown, S. L., Cifuentes, E. F., Čiliak, M., Contador, T., Convey, P., Cooper, E. J., Cremonese, E., Curasi, S. R., Curtis, R., Cutini, M., Dahlberg, C. J., Daskalova, G. N., de Pablo, M. A., Della Chiesa, S., Dengler, J., Deronde, B., Descombes, P., Di Cecco, V., Di Musciano, M., Dick, J., Dimarco, R. D., Dolezal, J., Dorrepaal, E., Dušek, J., Eisenhauer, N., Eklundh, L., Erickson, T. E., et al.: Global maps of soil temperature, Global Change Biology, 28, 3110–3144, https://doi.org/10.1111/gcb.16060, 2022.

Lenoir, J. and Svenning, J.-C.: Climate-related range shifts - a global multidimensional synthesis and new research directions, Ecography, 38, 15–28, https://doi.org/10.1111/ecog.00967, 2015.

Lindsay, J. B.: Whitebox GAT: A case study in geomorphometric analysis, Computers and Geosciences, 95, 75–84, https://doi.org/10.1016/j.cageo.2016.07.003, 2016.

Lindsay, J. B. and Creed, I. F.: Distinguishing actual and artefact depressions in digital elevation data, Computers & Geosciences, 32, 1192–1204, https://doi.org/10.1016/j.cageo.2005.11.002, 2006.

Lindsay, J. B. and Dhun, K.: Modelling surface drainage patterns in altered landscapes using LiDAR, International Journal of Geographical Information Science, 29, 397–411, https://doi.org/10.1080/13658816.2014.975715, 2015.

Ludwig, M., Moreno-Martinez, A., Hölzel, N., Pebesma, E., and Meyer, H.: Assessing and improving the transferability of current global spatial prediction models, Global Ecology and Biogeography, 32, 356–368, https://doi.org/10.1111/geb.13635, 2023.

Lundquist, J. D. and Huggett, B.: Evergreen trees as inexpensive radiation shields for temperature sensors, Water Resources Research, 44, W00D04, https://doi.org/10.1029/2008WR006979, 2008.

Macek, M., Kopecký, M., and Wild, J.: Maximum air temperature controlled by landscape topography affects plant species composition in temperate forests, Landscape Ecology, 34, 2541–2556, https://doi.org/10.1007/s10980-019-00903-x, 2019.

Macek, M., Man, M., Brůna, J., Hederová, L., Klinerová, T., Prošek, J., Růžičková, A., Wild, J., and Kopecký, M.: CzechGrids Micro, , https://doi.org/10.5281/zenodo.18472086, 2026.

Maclean, I. M. D., Duffy, J. P., Haesen, S., Govaert, S., De Frenne, P., Vanneste, T., Lenoir, J., Lembrechts, J. J., Rhodes, M. W., and Van Meerbeek, K.: On the measurement of microclimate, Methods in Ecology and Evolution, 12, 1397–1410, https://doi.org/10.1111/2041-210X.13627, 2021.

Man, M., Macek, M., Brůna, J., Hederová, L., Klinerová, T., Růžičková, A., Prošek, J., and Kopecký, M.: Atlas of the forest microclimate in Bohemian and Saxon Switzerland, 2022a.

Man, M., Wild, J., Macek, M., and Kopecký, M.: Can high-resolution topography and forest canopy structure substitute microclimate measurements? Bryophytes say no, Science of The Total Environment, 821, 153377, https://doi.org/10.1016/j.scitotenv.2022.153377, 2022b.

Man, M., Kalčík, V., Macek, M., Brůna, J., Hederová, L., Wild, J., and Kopecký, M.: <scp> *myClim* </scp> : Microclimate data handling and standardised analyses in R, Methods in Ecology and Evolution, 14, 2308–2320, https://doi.org/10.1111/2041-210X.14192, 2023.

Meineri, E. and Hylander, K.: Fine-grain, large-domain climate models based on climate station and comprehensive topographic information improve microrefugia detection, Ecography, 40, 1003–1013, https://doi.org/10.1111/ecog.02494, 2017.

Muñoz-Sabater, J., Dutra, E., Agustí-Panareda, A., Albergel, C., Arduini, G., Balsamo, G., Boussetta, S., Choulga, M., Harrigan, S., Hersbach, H., Martens, B., Miralles, D. G., Piles, M., Rodríguez-Fernández, N. J., Zsoter, E., Buontempo, C., and Thépaut, J.-N.: ERA5-Land: a state-of-the-art global reanalysis dataset for land applications, Earth System Science Data, 13, 4349–4383, https://doi.org/10.5194/essd-13-4349-2021, 2021.

Niittynen, P., Salminen, H., Peña-Aguilera, P., Aalto, J., Alahuhta, J., Luoto, M., Maliniemi, T., Rissanen, T., Roslin, T., Tukiainen, H., Tyystjärvi, V., and Kemppinen, J.: A Gridded Microclimate Dataset from a Sub-Arctic Biodiversity Hotspot in Finland, bioRxiv [preprint], https://doi.org/10.1101/2024.03.30.587419, 2024.

Nobre, A. D., Cuartas, L. A., Hodnett, M., Rennó, C. D., Rodrigues, G., Silveira, A., Waterloo, M., and Saleska, S.: Height Above the Nearest Drainage – a hydrologically relevant new terrain model, Journal of Hydrology, 404, 13–29, https://doi.org/10.1016/j.jhydrol.2011.03.051, 2011.

Pauls, J., Schrödter, K., Ligensa, S., Schwartz, M., Turan, B., Zimmer, M., Saatchi, S., Pokutta, S., Ciais, P., and Gieseke, F.: ECHOSAT: Estimating Canopy Height Over Space And Time, 2026.

Potter, K. a, Arthur Woods, H., and Pincebourde, S.: Microclimatic challenges in global change biology, Global Change Biology, 19, 2932–2939, https://doi.org/10.1111/gcb.12257, 2013.

R Core Team: R: A Language and Environment for Statistical Computing, 2025.

Rice, S. K., Gagliardi, T. A., and Krasa, R. A.: Canopy structure affects temperature distributions and free convection in moss shoot systems, 105, 1499–1511, https://doi.org/10.1002/ajb2.1145, 2018.

Rizwan, A. M., Dennis, L. Y. C., and Liu, C.: A review on the generation, determination and mitigation of Urban Heat Island, Journal of Environmental Sciences, 20, 120–128, https://doi.org/10.1016/S1001-0742(08)60019-4, 2008.

Roussel, J., Auty, D., Coops, N. C., Tompalski, P., Goodbody, T. R. H., Sánchez, A., Bourdon, J., Boissieu, F. D., and Achim, A.: lidR : An R package for analysis of Airborne Laser Scanning (ALS) data, Remote Sensing of Environment, 251, 112061, https://doi.org/10.1016/j.rse.2020.112061, 2020.

Simpson, G. L.: gratia : An R package for exploring generalized additive models, Journal of Open Source Software, 9, 1–10, https://doi.org/10.21105/joss.06962, 2024.

Song, J., Wang, J., Xia, X., Lin, R., Wang, Y., and Zhou, M.: Characterization of Urban Heat Islands Using City Lights : Insights from MODIS and VIIRS DNB Observations, 2021.

Tolan, J., Yang, H. I., Nosarzewski, B., Couairon, G., Vo, H. V., Brandt, J., Spore, J., Majumdar, S., Haziza, D., Vamaraju, J., Moutakanni, T., Bojanowski, P., Johns, T., White, B., Tiecke, T., and Couprie, C.: Very high resolution canopy height maps from RGB imagery using self-supervised vision transformer and convolutional decoder trained on aerial lidar, Remote Sensing of Environment, 300, 113888, https://doi.org/10.1016/j.rse.2023.113888, 2024.

Uxa, T.: When Statistical Learning Violates Physics: An Extensive Mismatch in Soil Temperature–Depth Relationships in Global Maps of Soil Temperature, Global Change Biology, 31, https://doi.org/10.1111/gcb.70574, 2025.

Valavi, R., Elith, J., Lahoz-Monfort, J. J., and Guillera-Arroita, G.: blockCV: An r package for generating spatially or environmentally separated folds for k-fold cross-validation of species distribution models, Methods in Ecology and Evolution, 10, 225–232, https://doi.org/10.1111/2041-210X.13107, 2019.

https://doi.org/10.5194/essd-2026-344
Preprint. Discussion started: 19 August 2026

Vandewiele, M., Geres, L., Lotz, A., Mandl, L., Richter, T., Seibold, S., Seidl, R., and Senf, C.: Mapping spatial microclimate patterns in mountain forests from LiDAR, Agricultural and Forest Meteorology, 341, 109662, https://doi.org/10.1016/j.agrformet.2023.109662, 2023.

Vanwalleghem, T. and Meentemeyer, R. K.: Predicting forest microclimate in heterogeneous landscapes, Ecosystems, 12, 1158–1172, https://doi.org/10.1007/s10021-009-9281-1, 2009.

Von Arx, G., Graf Pannatier, E., Thimonier, A., and Rebetez, M.: Microclimate in forests with varying leaf area index and soil moisture: Potential implications for seedling establishment in a changing climate, Journal of Ecology, 101, 1201–1213, https://doi.org/10.1111/1365-2745.12121, 2013.

Wickham, H.: ggplot2: Elegant Graphics for Data Analysis, Springer-Verlag, New York, 2016.

Wild, J., Kopecký, M., Macek, M., Šanda, M., Jankovec, J., and Haase, T.: Climate at ecologically relevant scales: A new temperature and soil moisture logger for long-term microclimate measurement, Agricultural and Forest Meteorology, 268, 40–47, https://doi.org/10.1016/j.agrformet.2018.12.018, 2019.

WMO: Guide to Instruments and Methods of Observation (WMO-No. 8), Volume I – Measurement of Meteorological Variables, World Meteorological Organisation, Geneva, 199–358 pp., https://doi.org/10.59327/WMO/CIMO/1, 2024.

Wood, S. N., Li, Z., Shaddick, G., and Augustin, N. H.: Generalized Additive Models for Gigadata: Modeling the U.K. Black Smoke Network Daily Data, Journal of the American Statistical Association, 112, 1199–1210, https://doi.org/10.1080/01621459.2016.1195744, 2017.

Zellweger, F., Coomes, D., Lenoir, J., Depauw, L., Maes, S. L., Wulf, M., Kirby, K. J., Brunet, J., Kopecký, M., Máliš, F., Schmidt, W., Heinrichs, S., den Ouden, J., Jaroszewicz, B., Buyse, G., Spicher, F., Verheyen, K., and De Frenne, P.: Seasonal drivers of understorey temperature buffering in temperate deciduous forests across Europe, Global Ecology and Biogeography, 28, 1774–1786, https://doi.org/10.1111/geb.12991, 2019.

Zellweger, F., Sulmoni, E., Malle, J. T., Baltensweiler, A., Jonas, T., Zimmermann, N. E., Ginzler, C., Karger, D. N., De Frenne, P., Frey, D., and Webster, C.: Microclimate mapping using novel radiative transfer modelling, Biogeosciences, 21, 605–623, https://doi.org/10.5194/bg-21-605-2024, 2024.

Zevenbergen, L. W. and Thorne, C. R.: Quantitative analysis of land surface topography, Earth Surface Processes and Landforms, 12, 47–56, https://doi.org/10.1002/esp.3290120107, 1987.